Low Cost and Waste Materials for Water Treatment

Science and Technology Program
Research and Development Office
Final Report No. ST-2020-1785

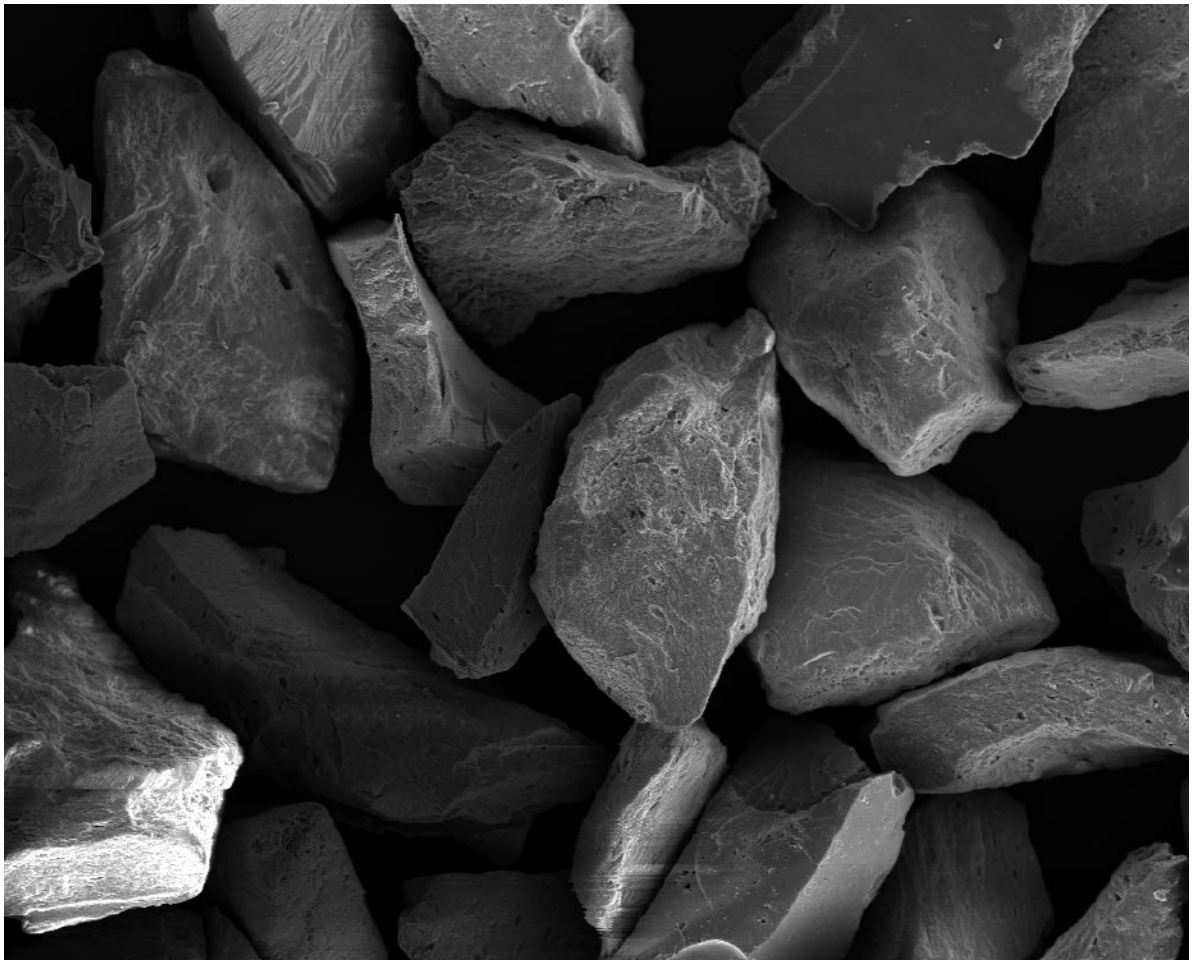

REPORT DOCUMENTATION PAGE

Form Approved
OMB No. 0704-0188

1. REPORT DATE *(DD-MM-YYYY)*	2. REPORT TYPE	3. DATES COVERED *(From - To)*
17-08-2020	Research	October 2017 – August 2020

4. TITLE AND SUBTITLE	
Low Cost and Waste Materials for Water Treatment	5a. CONTRACT NUMBER WBS: RR4888FARD1802501 WOID: FA865
	5b. GRANT NUMBER
	5c. PROGRAM ELEMENT NUMBER 1541 (S&T)
6. AUTHOR(S) Anthony Kennedy, Ph.D., P.E., Civil Engineer Miguel Arias-Paic, Ph.D., P.E., Civil Engineer	5d. PROJECT NUMBER ST-2020-1785
	5e. TASK NUMBER
	5f. WORK UNIT NUMBER

7. PERFORMING ORGANIZATION NAME(S) AND ADDRESS(ES)	8. PERFORMING ORGANIZATION REPORT NUMBER
US Bureau of Reclamation Denver Federal Center Building 67 6th Ave & Kipling St Denver CO 80225	
9. SPONSORING/MONITORING AGENCY NAME(S) AND ADDRESS(ES)	10. SPONSOR/MONITOR'S ACRONYM(S)
Science and Technology Program Research and Development Office Bureau of Reclamation U.S. Department of the Interior Denver Federal Center PO Box 25007, Denver, CO 80225-0007	Reclamation
	11. SPONSOR/MONITOR'S REPORT NUMBER(S) ST-2020-1785

12. DISTRIBUTION/AVAILABILITY STATEMENT
Final Report may be downloaded from https://www.usbr.gov/research/projects/index.html

13. SUPPLEMENTARY NOTES

14. ABSTRACT
Overall, this study consisted of three case studies for exploring low cost and waste materials for water treatment. The first case study investigated the use of biochar for the removal of metals from mine drainage water at the Leadville Mine Drainage Tunnel (LMDT) water treatment plant (WTP), a United States Bureau of Reclamation (USBR) owned facility, near Leadville, Colorado. The second case study investigated the use of bone char for the removal of fluoride from groundwater near the City of Lawton, Oklahoma. The third case study investigated the use of waste steel slag (WSS) for the removal of metals from mine drainage water at the LMDT WTP.

15. SUBJECT TERMS
biochar, bone char, steel slag, impaired waters, water treatment

16. SECURITY CLASSIFICATION OF:			17. LIMITATION OF ABSTRACT	18. NUMBER OF PAGES	19a. NAME OF RESPONSIBLE PERSON
a. REPORT	b. ABSTRACT	THIS PAGE		57	Anthony Kennedy
U	U	U			19b. TELEPHONE NUMBER *(Include area code)* 303-445-3230

Standard Form 298 (Rev. 8/98)
Prescribed by ANSI Std. Z39.18

Mission Statements

The Department of the Interior (DOI) conserves and manages the Nation's natural resources and cultural heritage for the benefit and enjoyment of the American people, provides scientific and other information about natural resources and natural hazards to address societal challenges and create opportunities for the American people, and honors the Nation's trust responsibilities or special commitments to American Indians, Alaska Natives, and affiliated island communities to help them prosper.

The mission of the Bureau of Reclamation is to manage, develop, and protect water and related resources in an environmentally and economically sound manner in the interest of the American public.

Disclaimer

Information in this report may not be used for advertising or promotional purposes. The data and findings should not be construed as an endorsement of any product or firm by the Bureau of Reclamation, Department of Interior, or Federal Government. The products evaluated in the report were evaluated for purposes specific to the Bureau of Reclamation mission. Reclamation gives no warranties or guarantees, expressed or implied, for the products evaluated in this report, including merchantability or fitness for a particular purpose.

Acknowledgements

The Science and Technology Program, Bureau of Reclamation, sponsored this research. The authors would like to thank Leadville Mine Drainage Tunnel staff and plant manager, Jenelle Stefanic; Alejandro Caicedo for slag samples; Matt Bentley for biochar samples; City of Lawton staff; Great Plains Technology Center staff; Garver staff; Nathan Kuhnert and Collins Balcombe from the Oklahoma-Texas Area Office.

Low Cost and Waste Materials for Water Treatment

Final Report No. ST-2020-1785

prepared by

Technical Service Center
Water Treatment Group
Anthony Kennedy, Ph.D., P.E., Civil Engineer
Miguel Arias-Paic, Ph.D., P.E., Civil Engineer

Peer Review

Bureau of Reclamation
Research and Development Office
Science and Technology Program

Final Report No. ST-2020-1785

Low Cost and Waste Materials for Water Treatment

ANTHONY KENNEDY
Digitally signed by ANTHONY KENNEDY
Date: 2020.08.17 13:16:02 -06'00'

Prepared by: Anthony Kennedy, Ph.D., P.E.
Civil Engineer

LEAH FLINT
Digitally signed by LEAH FLINT
Date: 2020.08.18 08:57:55 -06'00'

Peer Review by: Leah Flint
Civil Engineer

"This information is distributed solely for the purpose of pre-dissemination peer review under applicable information quality guidelines. It has not been formally disseminated by the Bureau of Reclamation. It does not represent and should not be construed to represent Reclamation's determination or policy."

Acronyms and Abbreviations

AA	Activated Alumina
BC	Bone Char
BV	Bed Volume
DI	Deionized
EBCT	Empty Bed Contact Time
EPA	Environmental Protection Agency
GAC	Granular Activated Carbon
LMDT	Leadville Mine Drainage Tunnel
PD	Proportional Diffusivity
RSSCT	Rapid Small-Scale Column Test
ST	Specific Throughput
UR	Use Rate
USBR	US Bureau of Reclamation
WTP	Water Treatment Plant

Measurements

°C	degree Celcius
g	gram
mg/L	milligrams per liter

Executive Summary

Overall, this study consisted of three case studies for exploring low cost and waste materials for water treatment. The first case study investigated the use of biochar for the removal of metals from mine drainage water at the Leadville Mine Drainage Tunnel (LMDT) water treatment plant (WTP), a United States Bureau of Reclamation (USBR) owned facility, near Leadville, Colorado. The second case study investigated the use of bone char for the removal of fluoride from groundwater near the City of Lawton, Oklahoma. The third case study investigated the use of steel slag for the removal of metals from mine drainage water at the LMDT WTP.

Case Study No. 1 – Biochar for Metals Removal

A total of 10 different biochars were tested in powdered form to evaluate metals removal from raw water at the LDMT WTP. Overall, removal was very poor at biochar doses ranging from 1 to 1,000 mg/L, with no removal passing 50% based on analysis of cadmium (Cd), manganese, (Mn), and zinc (Zn). As such, testing ceased to focus on Case Study No. 3.

Case Study No. 2 – Bone Char for Fluoride Removal

Bone char was found to be effective at removing fluoride from groundwater and potentially competitive against a best available technology, activated alumina. Journal of Environmental Engineering pre-proof manuscript is attached.

Case Study No. 3 – Steel Slag for Metals Removal

Powdered basic oxygen furnace steel slag was found to be effective at removing metals from mine drainage water and potentially competitive against widely used chemicals, lime and sodium hydroxide. Journal of Water Process Engineering pre-proof manuscript is attached.

Contents

Page
Mission Statements ..... **ii**
Disclaimer ..... **ii**
Acknowledgements ..... **ii**
Peer Review ..... **iii**
Acronyms and Abbreviations ..... **iv**
Measurements ..... **iv**
Executive Summary ..... **v**
Case Study No. 1 – Biochar for Metals Removal v
Case Study No. 2 – Bone Char for Fluoride Removal v
Case Study No. 3 – Steel Slag for Metals Removal v
Case Study No. 1 – Biochar for Metals Removal **7**
Background 7
Materials and Methods 7
Results, Discussion, and Conclusions 9
References 11
Case Study No. 2 – Bone Char for Fluoride Removal **12**
Case Study No. 3 – Steel Slag for Metals Removal **13**
Recommended Next Steps **13**
Appendix A **14**
Appendix B **38**

Case Study No. 1 – Biochar for Metals Removal

Background

Biochar, which is a low-cost, relatively high surface area material made from the pyrolysis of organic feedstocks (e.g., pine, nut shells, husks, manure, etc.), has recently gained attention as an adsorptive media for water treatment. Specifically, biochar has been tested for the removal of both organic (e.g., pesticides) and inorganic (e.g., metals) contaminants from water, with the goal of providing a potential alternative to conventional media such as activated carbon or ion exchange resins. Several recent reviews documenting biochar research for metals removal have shown promise, both with and without modifications to typical biochar production conditions (Mohan et al. 2014, Tan et al. 2015, Inyang et al. 2016, Li et al. 2017). Removal mechanisms for metals onto biochar surfaces include ion exchange, electrostatic attraction, surface complexation, physical adsorption, and co-precipitation. As such, highly functionalized biochar surfaces are desirable, but must be balanced against high pyrolysis temperatures that can achieve higher surface areas. Considering USBR owns and operates the LMDT WTP with the purpose of removing total and dissolved metals from the Environmental Protection Agency's (EPA) California Gulch Superfund Site (Operable Unit 6) drainage water, biochar was tested a potential alternative to the current treatment process.

Materials and Methods

Average raw water quality parameters at the LMDT WTP is shown in Table 1 and includes only the metals cadmium (Cd), manganese (Mn), and zinc (Zn) as these are the most difficult to remove using conventional precipitation and oxidation processes. Alkalinity was measured by titration with sulfuric acid (Method 8203, Hach, Colorado). pH and temperature were measured using a gel-filled electrode (Intellical™ PHC101, Hach, Colorado) attached to a portable multi-meter (HQ40d, Hach, Colorado), calibrated daily. Cd, Mn, and Zn were measured by a certified, commercial laboratory (Green Analytical Laboratories, Colorado) under contract number 140R8118P0031 according to EPA Method 200.8, with minimum reporting limits of 0.0001, 0.0005, and 0.002 mg/L, respectively.

Table 1. Average LMDT WTP raw water quality during testing.

Parameter	Average±Standard Deviation	Units
Alkalinity	145±5	mg/L as $CaCO_3$
pH	7.0±0.1	su
Temperature	11±1	°C
Cd	0.007±0.001	mg/L
Mn	1.1±0.2	mg/L
Zn	1.9±0.2	mg/L

29 All 10 biochars that were tested are shown in Table 2 in addition to details related to feedstock,
30 manufacturer, and pyrolysis conditions. Two pine biochars were purchased directly from Biochar
31 Now, LLC, and Confluence Energy, LLC. Eight other biochars, four pine and four biosolids, were
32 contracted out to the R. Scott Summers Research Group at the University of Colorado – Boulder
33 under contract number 140R8118P0054. For ash-treated biochars, ash was first created from pine or
34 biosolids by heating them in uncovered crucibles to 550°C in a muffle furnace for 2 hours. Ash was
35 dissolved in deionized (DI) water (>16 MΩ) for 30 minutes at 2,000 mg/L and then filtered to
36 remove remaining solids. Feedstocks were then soaked at a 1:100 ash to feedstock dry mass ratio
37 and dried overnight at 110°C. Pyrolysis was carried out in a muffle furnace using covered crucibles.
38 Following pyrolysis, each biochar was carefully ground by hand using a mortar and pestle and
39 vibratory sieve shaker (EW-59986-03, Cole-Parmer, Illinois). Biochar less than 75 µm, or No. 200
40 standard sieve mesh size, was collected and added to deionized water (>16 MΩ) to create 20,000
41 mg/L slurries in 250 mL amber glass bottles.
42
43 *Table 2. Biochars tested.*

Biochar Designation	Feedstock	Manufacturer	Pyrolysis Conditions
Biochar Now	pine	Biochar Now, LLC (www.biocharnow.com/)	550 to 600°C for 8 to 12 hours
Confluence Energy	pine	Confluence Energy, LLC (www.confluenceenergy.com/)	300 to 700°C For 15 minutes
Pine (400°C)	pine	University of Colorado – Boulder R. Scott Summers Research Group (www.colorado.edu/faculty/summers/research)	400°C for 2 hours
Pine (800°C)	pine		800°C for 2 hours
Ash-Treated Pine (400°C)	pine		400°C for 2 hours
Ash-Treated Pine (800°C)	pine		800°C for 2 hours
Biosolids (400°C)	biosolids		400°C for 2 hours
Biosolids (800°C)	biosolids		800°C for 2 hours
Ash-Treated Biosolids (400°C)	biosolids		400°C for 2 hours
Ash-Treated Biosolids (800°C)	biosolids		800°C for 2 hours

44
45 To test the adsorption Cd, Mn, and Zn to the 10 different biochar surfaces, a jar tester with six, 2 L
46 jars was used (PB-900, Phipps & Bird, Virginia). Biochar was added as a slurry to raw water at doses
47 ranging from 1 to 1,000 mg/L during a 1-minute rapid mix stage (paddle speed: 300 rpm, average
48 velocity gradient (G): 300 to 400 s^{-1}). Biochar was suspended and in contact raw water during a 60-

minute slow mix stage (paddle speed: 60 rpm, G: 40 to 60 s^{-1}). At the end of mixing samples were immediately taken for pH, temperature, and dissolved metals after filtering through a 0.45 μm filter (Versapor 66408, Pall Corporation, New York) using a peristaltic pump and controller.

Results, Discussion, and Conclusions

Cd, Mn, and Zn normalized dissolved concentrations as function of biochar dose are shown in Figure 1, Figure 2, and Figure 3, respectively. For all metals removal was minimal, even at the highest dose of 1,000 mg/L. On a normalized basis, or the effluent concentration (C) divided by the average influent concentration (C_0), Cd was removed the most at almost 50% at a dose 1,000 mg/L using the ash-treated biosolids biochar. It was expected the biosolids biochar would have a higher functionalized surface compared to pine, but removal was still somewhat disappointing. The results of this study draw into question recent pushes for the use of biochar for metals removal. Certainly, biochar is a cheap material and can contribute to carbon sequestration, however, from the figures below it can be seen that very high doses are required, consistent with the previously mentioned reviews. As such, work on this case study ceased and efforts were diverted to Case Study No. 3.

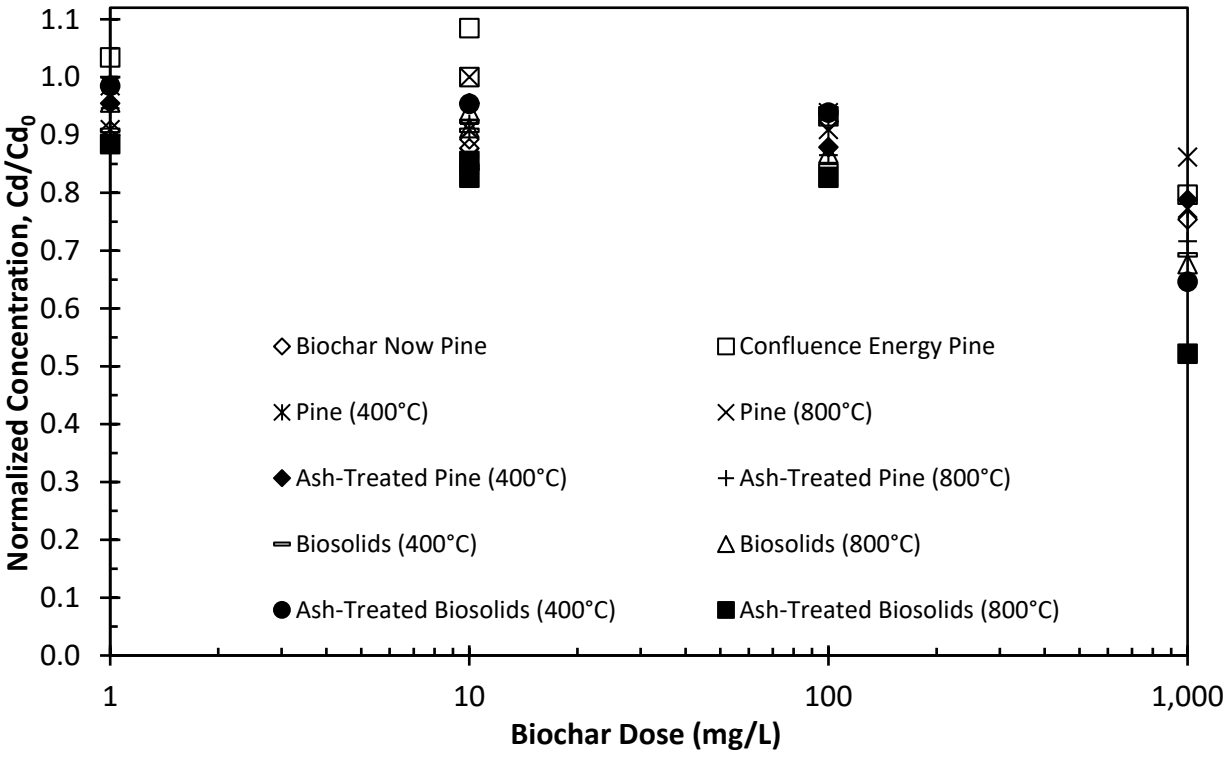

Figure 1. Normalized dissolved Cd concentration as a function of biochar dose.

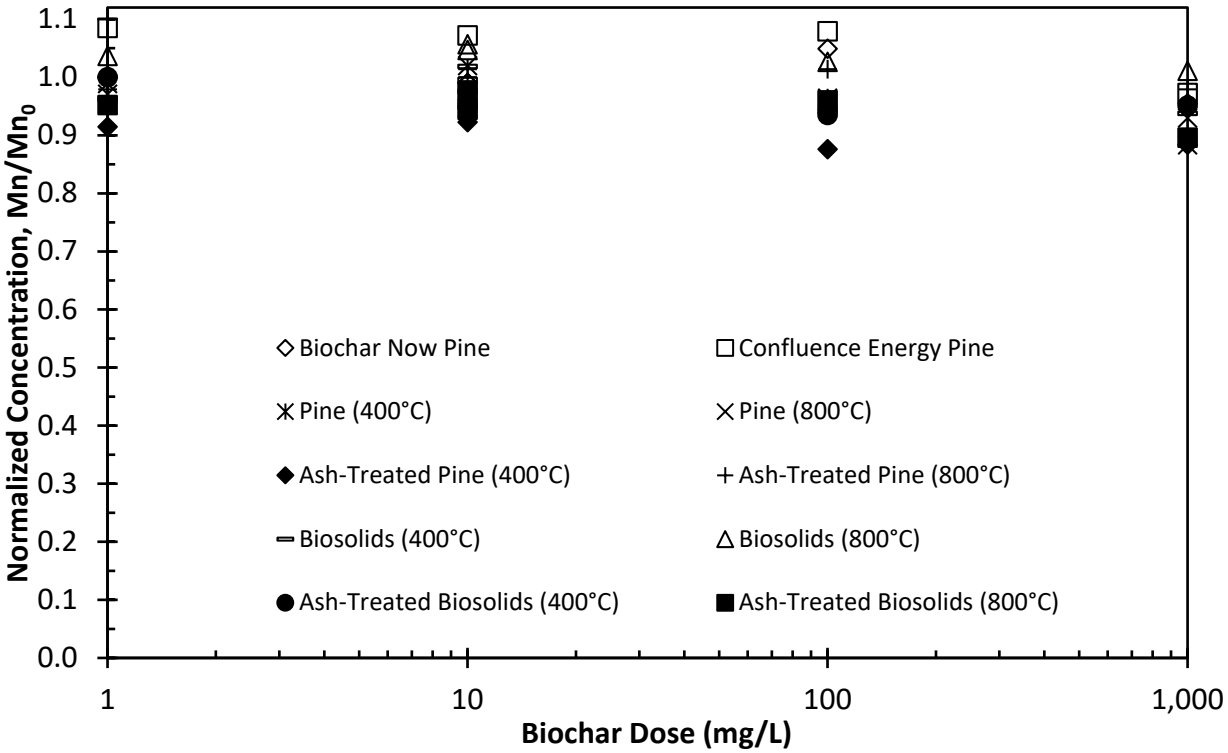

Figure 2. Normalized dissolved Mn concentration as a function of biochar dose.

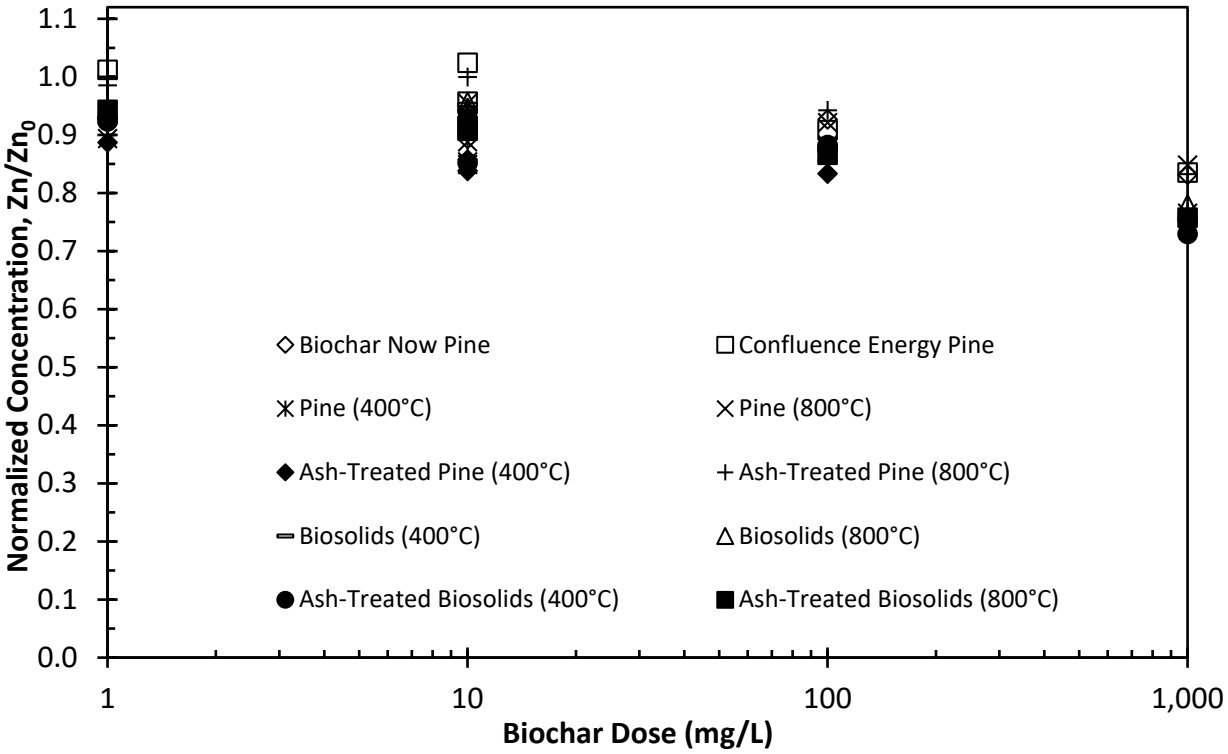

Figure 3. Normalized dissolved Zn concentration as a function of biochar dose.

References

Inyang, M.I., Gao, B., Yao, Y., Xue, Y., Zimmerman, A., Mosa, A., Pullammanappallil, P., Ok, Y.S., and Cao, X. 2016. A review of biochar as a low-cost adsorbent for aqueous heavy metal removal. *Critical Reviews in Environmental Science and Technology*, 46:406-433.

Li, H., Dong, X., da Silva, E.B., de Oliveira, L.M., Chen, Y., and Ma, L.Q. 2017. Mechanisms of metal sorption by biochars: Biochar characteristics and modifications. *Chemosphere*, 178:466-478.

Mohan, D., Sarswat, A., Ok, Y.S., and Pittman Jr., C.U. 2014. Organic and inorganic contaminants rmeoval from water with biochar, a renewable, low cost and sustainable adsorbent – A critical review. *Bioresource Technology*, 160:191-202.

Tan, X., Liu, Y., Zeng, G., Wang, X., Hu, X., Gu, Y., and Yang, Z. 2015. Application of biochar for the removal of pollutants from aqueous solutions. *Chemosphere*, 125:70-85.

Case Study No. 2 – Bone Char for Fluoride Removal

See Appendix A for the pre-proof manuscript accepted to the Journal of Environmental Engineering (www.ascelibrary.org/journal/joeedu). The following also resulted from this project:

- In conjunction with Garver, the City of Lawton, Oklahoma, used activated alumina breakthrough data for fluoride to evaluate treatment alternatives to expand the city's water supplies
- USBR was contacted by reGENESIS Consulting Services, LLC, in Hanover, Pennsylvania, for insights related to the use of bone char for a bottled water project in Utah
- Funds were provided to an assistant professor of civil engineering at Gonzaga University in Spokane, Washington, to further evaluate bone char production conditions to potentially enhance fluoride removal to match activated alumina performance
- USBR was invited to collaborate with an assistant professor of civil, construction, and environmental engineering at North Carolina State University in Raleigh, North Carolina, on other bone char-fluoride related research projects
- Presentations at professional conferences

Case Study No. 3 – Steel Slag for Metals Removal

See Appendix B for the pre-proof manuscript accepted to the Journal of Water Process Engineering (https://www.journals.elsevier.com/journal-of-water-process-engineering). The following also resulted from this project:

- Presentations at professional conferences

Recommended Next Steps

Next steps include securing more research funding to further investigate the use of bone char for fluoride and steel slag for metals removal from water.

Appendix A

Journal of Environmental Engineering – Accepted, Pre-Proof Manuscript

Fixed-Bed Adsorption Comparisons of Bone Char and Activated Alumina for the Removal of Fluoride from Drinking Water

Anthony M. Kennedy and Miguel Arias-Paic

Abstract

Fluoride is commonly found at elevated concentrations in groundwaters worldwide and is difficult to remove even with activated alumina (AA) adsorption, the best available technology. Consequently, alternative treatment technologies for fluoride removal continue to be researched including the use of bone char (BC) adsorption. However, BC studies are limited mostly to batch or equilibrium studies, which can be difficult to extend to full-scale applications. Therefore, the goal of this study was to compare a BC to a commercial AA for treating a groundwater with a naturally-occurring fluoride concentration of 8.5 mg/L using pilot- and bench-scale fixed-bed adsorption tests. At the pilot-scale using an empty bed contact time (EBCT) of 10 minutes, fluoride breakthrough reached 1.5 mg/L within 450 bed volumes (3.1 days) and 650 bed volumes (4.5 days) for BC and AA, respectively. Two designs of the rapid small-scale column test (RSSCT) were applied to simulate the pilot columns, where the proportional diffusivity (PD-RSSCT) design provided a more adequate prediction of fluoride breakthrough to 1.5 mg/L. The PD-RSSCT was also used to evaluate BC and AA EBCTs of 10 and 20 minutes, with the longer EBCT providing no significant increase in adsorbent use efficiency. Complete BC regeneration using countercurrent flow to the PD-RSSCT was limited by exposure to the sodium hydroxide regenerant solution and potentially the presence of arsenic.

Introduction

Fluoride is present in most drinking waters from natural sources, due to weathering or leaching of fluoride-containing rocks and soils but may also be present from anthropogenic sources such as its addition for public health protection (prevention of dental caries), and/or contamination from industrial or agricultural activity (Fawell et al. 2006; Ayoob et al. 2008). The concentration of fluoride in drinking water has been extensively studied and debated for decades (NRC 2006), and despite longstanding regulations or guidelines, remains somewhat unresolved. What is certain however, is that high concentrations (>4 mg/L) of fluoride in drinking water can cause detrimental health effects such as dental or skeletal fluorosis in humans (Fawell et al. 2006; NRC 2006; Ayoob et al. 2008). Limits for fluoride in drinking water typically follow either the (1) United States Environmental Protection Agency (EPA) maximum contaminant level (MCL) of 4.0 mg/L (albeit rarely), (2) EPA secondary MCL of 2.0 mg/L, (3) World Health Organization (WHO) guideline of 1.5 mg/L (WHO 2017), or (4) United States Public Health Service (PHS) recommendation of 0.7 mg/L (PHS 2015). The WHO guideline is perhaps the most commonly used in practice and fluoride-related water research. For example, it was used as the benchmark for worldwide geogenic fluoride occurrence study (Amini et al. 2008), which highlighted the water-stressed western United States as a region with significant fluoride occurrence in groundwater.

As a free ion in water, fluoride is a relatively difficult to remove due to its monovalent charge, small molar mass, and high solubility, ~40,000 mg/L for sodium fluoride (NaF) at 25°C (Haynes et al. 2016). Several fluoride removal processes such as coagulation, adsorption, ion

exchange, electrochemical-based, and membrane-based have been studied and/or implemented with varying success (Ayoob et al. 2008; EPA 2014). For centralized treatment systems, adsorption using activated alumina (AA) has been identified as the best available treatment technology for fluoride removal (Clifford et al. 2011; EPA 2014). AA is primarily comprised of aluminum oxide (Al_2O_3), which upon hydration forms $\underline{Al}OH_2^+$ (pH<6) and $\underline{Al}OH$ (pH>7) surface hydroxo groups (Hao and Huang 1986). Fluoride adsorbs to the AA surface through ligand exchange, whereby depending on pH, a hydroxide ion (OH^-) or water molecule (H_2O) is released from the AA surface and $\underline{Al}F$, and potentially $\underline{Al}F_2^-$, is formed (Hao and Huang 1986). Experimentally and in practice, it has been determined the optimal pH for fluoride adsorption is between 5 and 6 (Hao and Huang 1986; Clifford et al. 2011; EPA 2014), typically lowered using sulfuric acid (H_2SO_4) prior to entering an AA adsorber system. In terms of adsorbent use rate (UR), AA can be regenerated using 1 to 4% sodium hydroxide (NaOH) solutions to near full recovery of the initial fluoride adsorption capacity (Clifford et al. 1991; Clifford et al. 2011; EPA 2014).

As an alternative adsorbent to AA, bone char (BC) has been investigated and implemented in the past for both its affinity for fluoride and environmental appeal of using a waste product from one industry (e.g., cattle ranching) as a useful product for another. As far back as 1953, BC was implemented in full-scale adsorbers for fluoride removal, but was phased out due to cost and increased use of AA (Sorg 1978). By mass, BC consists of approximately 70% calcium phosphate ($Ca_3(PO_4)_2$) including hydroxyapatite ($Ca_{10}(PO_4)_6(OH)_2$); the structural component of bone (Medellin-Castillo et al. 2007; Ayoob 2008; EPA 2014; Rojas-Mayorga et al. 2015). Similar to AA, it has been proposed fluoride adsorbs to the BC surface through ligand exchange with hydroxyapatite hydroxide groups (Fan et al. 2003; Ayoob et al. 2008; Medellin-Castillo et al. 2016), ionic exchange with phosphate groups (Abe et al. 2004), and/or electrostatic attraction to $\underline{Ca}OH_2^+$ or $\underline{P}OH_2^+$ surface groups (Medellin-Castillo et al. 2016). BC has also been shown to be regenerable using sodium hydroxide (Sorg 1978, Medellin-Castillo et al. 2007; Yami et al. 2017).

Following the recent trends of increased biochar research for water treatment in both developed and developing communities, in addition to recognizing that freshwater supplies requiring only conventional treatment technologies are decreasing, there has been a resurgence in BC investigations for the adsorption of fluoride (Abe et al. 2004; Medellin-Castillo et al. 2007; Leyva-Ramos et al. 2010; Rojas-Mayorga et al. 2008; Brunson and Sabatini 2014; Medellin-Castillo et al. 2016; Nigri et al. 2017; Yami et al. 2017; Kearns et al. 2018). Most studies have evaluated BC(s) without direct comparisons to AA and/or used batch or isotherm studies. Comparisons to AA are useful for benchmarking BC performance to the best available technology. Batch studies are useful for relative comparisons and absorbability testing, but they do not project full-scale adsorber performance (e.g., throughput, runtimes, regeneration frequency, etc.).

To better project full-scale adsorber performance (i.e., generation of breakthrough curves), the rapid small-scale column test (RSSCT) was developed by Crittenden et al. (1986a, 1987, 1991) for granular activated carbon (GAC) adsorption of dissolved organics constituents. The basis for the RSSCT is similitude between the dimensionless numbers of the dispersed-flow pore and surface diffusion model, which includes the mass transport mechanisms of advection, dispersion, external (film) diffusion, and internal (intraparticle) diffusion (Crittenden et al. 1986b). Based on this dimensional analysis, simple scaling equations were developed relating the empty bed contact time (EBCT) and hydraulic loading rate (HLR) to the GAC particle sizes, or mean GAC particle diameters (d_p), of the large column (LC – i.e., pilot or full-scale) and small column (SC – i.e., RSSCT). These relationships assume GAC properties (void fractions, bulk densities, and adsorption capacities) remain relatively constant between the LC and SC. Although RSSCTs have proven useful for predicting organic constituent removal, they commonly require matching pilot studies or breakthrough result adjustments to provide accurate full-scale breakthrough predictions (Crittenden

et al. 1991; Corwin and Summers 2010; Summers et al. 2011; Crittenden et al. 2012; Kennedy et al. 2017). With some success, RSSCTs have been extended to other high specific surface area adsorbents with similar mass transfer processes to GAC, such as granular ferric hydroxide (GFH) adsorption of arsenate (Westerhoff et al. 2005) or tin-based nanoparticle adsorption of hexavalent chromium (Kaprara et al. 2017). However, the RSSCT has not been extended to AA in published literature and its use for BC or biochar has been limited.

Brunson and Sabatini (2014) did extend the RSSCT to BC and fluoride using the constant diffusivity design of the RSSCT (CD-RSSCT). Good agreement was observed between the LC (d_p=0.64 mm) and SC (d_p=0.30 mm) breakthrough curves, but further validation of the RSSCT was recommended. The study also compared BC and AA CD-RSSCT breakthrough curves, but the particles sizes were different at 0.13 and 0.30 mm, respectively, with the same column dimensions and media volume. The AA used showed much earlier breakthrough than expected based on other AA studies for the removal of fluoride (Clifford et al. 1991; Clifford et al. 2011; EPA 2014). Although they did not specifically use the RSSCT, Rojas-Mayorga et al. (2015) did use micro-columns to obtain fluoride breakthrough curves, but with the purpose of evaluating modeling approaches, not for predicting full-scale adsorber breakthrough.

BC comparisons to commercially-available AA, specifically fixed-bed adsorber studies are lacking, both of which are necessary to determine the feasibility of BC for the removal of fluoride from drinking water. Such design information would be useful for drinking water sources requiring fluoride removal, either for source diversification or lack of other source options (e.g., Clifford et al. 1991). The objectives of this study, as they relate to the adsorption of fluoride, were to (1) compare BC to AA using fixed-adsorbers with full-scale particle sizes (i.e., pilot columns), (2) further investigate the RSSCT for BC including regeneration, (3) evaluate extending the RSSCT to AA, and (4) evaluate adsorber operational parameters for both BC and AA using the RSSCT.

Methods and Materials

Water Quality and Analysis

Groundwater from a well located in southwest Oklahoma was periodically collected and shipped in opaque 200 L high-density polyethylene barrels to Denver, Colorado, for testing. Water was stored at room temperature (~20-23°C) prior to testing at the same temperature. Average raw groundwater quality is shown in Table 1 and was relatively consistent across all sampling events and during sample storage. Specifically, the raw groundwater fluoride concentration (C_0) was constant at approximately 8.5±0.2 mg/L, nearly six times the WHO guideline value of 1.5 mg/L, while all other measured water quality parameters were typical of a groundwater used as a drinking water source. It is important to note adsorption breakthrough curves are a function of C_0, with lower C_0 values resulting in longer adsorber runtimes. A C_0 value of 8.5 mg/L is on the higher range of what exists in the published AA literature (Clifford et al. 2011; EPA 2014) but very similar to recent BC work (Brunson and Sabatini 2014; Yami et al. 2017; Kearns et al. 2018).

Alkalinity, pH, temperature, and fluoride were measured for every test. For source water characterization, dissolved organic carbon (DOC), hardness, sulfate, total dissolved solids (TDS), and ultraviolet absorption at 254 nm (UVA_{254}) were done internally or externally by a certified laboratory according to Standard Method 5310C, Standard Method 2340B, EPA 300.0, EPA 160.1, and Standard Method 5910, respectively. Alkalinity was measured by titration with sulfuric acid (H_2SO_4) (Method 8203, Hach, Loveland, CO). pH was measured using a gel-filled electrode (Intellical™ PHC101, Hach) attached to a portable multi-meter (HQ40d, Hach), calibrated daily. Fluoride was measured using an ion selective electrode with a non-refillable reference and built-in temperature sensor (Intellical™ ISEF121, Hach). Each fluoride sample consisted of adding a

257 combined ionic strength adjustor and buffer powder pillow to a 25 mL sample volume in a 50 mL
258 glass beaker. Samples were well mixed during measurement using a magnetic stir bar and plate.
259 Although the probe was capable of measuring fluoride concentrations between 0.01 and 19,000
260 mg/L, 1.00 and 10.0 mg/L standard solutions were used for daily calibrations. Periodically, the
261 probe was conditioned and cleaned using commercial fluoride toothpaste and isopropyl alcohol. To
262 verify fluoride electrode readings, 16 split samples were analyzed for fluoride by an external, certified
263 laboratory by EPA Method 300.0. Fluoride sample concentrations ranged from below the laboratory
264 reporting limit of 0.1 mg/L up to C_0 (Table 1) and agreed well with probe measurements (R^2=0.97,
265 paired t-test p=0.21).
266
267 **Adsorbents**
268 A single, 1 kg batch of cattle-based BC (Confluence Energy, Kremmling, CO) was used for all BC
269 testing. As a proprietary product specific pyrolysis conditions were not available, but in short, a high
270 surface and porous structure was created from raw cattle bones pyrolyzed in a biochar retort for
271 approximately 8 hours at temperatures ranging from 350 to 650°C. It should be noted that over
272 such a wide pyrolysis temperature range, biochar surface area can change significantly, by factor of
273 three on average (Lehmann and Joseph 2015). As received, the BC was not sieved and ranged in size
274 from fines to greater than 1 cm. For testing, BC was carefully ground using a mortar and pestle and
275 wet-sieved with deionized water to 12x40, 60x80, and 100x200 US Standard mesh size fractions,
276 corresponding to natural logarithmic mean d_p values of 0.92, 0.21, and 0.11 mm, respectively. While
277 the large d_p value is common for full-scale GAC applications, the small d_p values are common to
278 RSSCT applications (Crittenden et al. 1991; Westerhoff et al. 2005; Corwin and Summers 2010;
279 Kennedy et al. 2017). Wet-sieving was accomplished using a low velocity stream of deionized water
280 (resistivity greater than 16 MΩ) distributed evenly across the sieve area. Deionized water was
281 periodically checked to ensure fluoride concentrations were below 0.1 mg/L as to not reduce the
282 BC's adsorption capacity for fluoride prior to testing.
283 A single, 1 kg batch of commercially-available AA (DD6, BASF Corporation, Florham Park,
284 NJ) was used for all AA testing. As a proprietary product specific production conditions were not
285 available, but in short, a high surface area and porous structure of aluminum oxide was created from
286 the dehydration of aluminum hydroxide ($Al(OH)_3$) at temperatures ranging from 300 to 600°C (EPA
287 2014). As received, the AA was pre-sieved to a 14x28 Tyler mesh size fraction, or a 16x30 US
288 Standard mesh size fraction, which corresponds to a natural logarithmic mean d_p value of 0.86 mm.
289 AA is also commonly available in the 28x48 Tyler mesh size fraction, or 30x50 US Standard mesh
290 size fraction with a logarithmic mean d_p value of 0.43 mm, but this size was not tested in this study.
291 Prior work has demonstrated both AA size fractions have similar adsorption capacity for fluoride,
292 but the smaller size fraction exhibits faster adsorption kinetics as observed through sharper
293 breakthrough curve profiles (Clifford et al. 1991). For testing in addition to the 16x30 (d_p=0.86 mm)
294 size fraction, AA US Standard mesh size fractions of 60x80 (d_p=0.21 mm) and 100x200 (d_p=0.11
295 mm) were made following the same procedure as for BC.
296 For visualization of the particle surface morphology and external pore openings as well as
297 elemental composition, both BC and AA were analyzed using scanning electron microscopy (SEM)
298 at 15 keV (JSM-6400, JEOL USA, Peabody, MA) coupled with energy-dispersive X-ray spectroscopy
299 (EDS) at a take-off angle of 35°. BC and AA samples were prepared by drying and sputter-
300 depositing 3 to 6 nm of elemental gold on approximately 1 cm^2 worth of media grains. EDS was
301 able to detect all elements except hydrogen, helium, lithium, and beryllium with a detection limit of
302 0.1%. Software (IXRF Systems, Inc., Austin, TX) was used to acquire EDS spectra in addition to
303 mass and atomic percent compositions.

BC and AA surface area and pore volume analyses were also performed on all particle sizes by a certified external laboratory (Micromeritics Instrument Corp., Norcross, GA) using both nitrogen gas (N_2) physisorption. Carbon dioxide gas (CO_2) physisorption was performed on the large particle sizes only. Both methods were chosen because of their application in the literature and documented N_2 diffusional problems for some biochars (Lehmann and Joseph 2015; Sigmund et al. 2017). Physisorption temperatures were -196 and 0°C for N_2 and CO_2, respectively, degassed at 200°C.

Pilot Column Tests

Design and operational parameters for the pilot columns are shown in Table 2 and were assumed to represent full-scale adsorbers because they used the same sieved BC or AA particle size (0.92 and 0.86 mm, respectively). Pilot columns were constructed from 25 mm nominal diameter (d_{bed}) schedule 40 clear polyvinyl chloride (PVC) pipe and fittings, fluorinated ethylene propylene (FEP) tubing, and polypropylene (PP) and stainless steel (SS) fittings. The PVC column size corresponded to a ratio of d_{bed} to d_p of approximately 27 and 29 for BC and AA, respectively, sufficient to avoid wall effects on mass transfer (Knappe et al. 1999). Noticeable fluoride adsorption to or desorption from fluorinated tubing was not observed. Water was fed to the pilot columns from 20 L glass carboys using a small diaphragm pump at a constant flow rate to reach the target operational values in Table 2.

An EBCT of 5 minutes is more typical for AA (Clifford et al. 1991; Clifford et al. 2011; EPA 2014), but an EBCT of 10 minutes was chosen for comparison to the unknown impact of EBCT on BC performance. An HLR of 1.0 m/h is below the typical range of 8 to 20 m/h (Clifford et al. 2011; EPA 2014) but was chosen to reduce the amount of water required, highlighting a drawback of piloting versus RSSCTs. This HLR is different than the relatively low HLR_{LC} value of 0.15 m/h used by Brunson and Sabatini (2014). Despite using a lower value, a HLR of 1.0 m/h still falls within the pure mechanical dispersion region associated with fixed-bed adsorbers in which dispersion effects on mass transfer are negligible. Quantitatively, the pure mechanical dispersion region has been empirically established by the product of the dimensionless Reynolds (Re) and Schmidt (Sc) numbers, or Re·Sc, falling between 200 and 200,000 (Crittenden et al. 1987; Westerhoff et al. 2005; Brunson and Sabatini 2014). As shown in Table 2, both BC and AA pilot columns had Re·Sc values greater than 400, assuming the diffusivity of fluoride in water (D_w) is approximately 1.5×10^{-5} cm^2/s at 25°C (Haynes et al. 2017).

BC or AA was loaded into a PVC column on a support layer of glass wool, then backwashed using deionized water to remove fines and achieve a settled bed length (L_{bed}) of 17 cm prior to starting each run. To minimize particulate-induced head loss across the column, a glass wool prefilter was placed just after the pump outlet and replaced regularly. With each addition of raw groundwater to the influent carboys, pH was adjusted to approximately 5.9 using laboratory grade 10 N sulfuric acid, within the typical operating range of 5.5 to 6.0 for AA operation (Hao and Huang 1986; Clifford et al. 2011; EPA 2014). Sulfuric acid addition to pH 5.9 reduced alkalinity to approximately 40 mg/L as $CaCO_3$. Samples for fluoride and pH were taken periodically from the influent and effluent of the pilot column. Pilot column runs were tested in duplicate to establish reproducibility.

Rapid Small-Scale Column Tests

Design and operational parameters for RSSCTs are shown in Table 2 and were designed to simulate the pilot columns according to the following equations for the CD-RSSCT, which assumes intraparticle diffusion coefficients (surface – D_s; and pore – D_p) of the target adsorbate are independent of d_p (Crittenden et al. 1986a; Crittenden et al. 1991),

$$EBCT_{SC} = EBCT_{LC} \cdot \left(\frac{d_{p,SC}}{d_{p,LC}}\right)^2 \quad \text{Eq. (1)}$$

$$HLR_{SC} = HLR_{LC} \cdot \frac{d_{p,LC}}{d_{p,SC}} \quad \text{Eq. (2)}$$

352 and the following equations for the PD-RSSCT, which assumes intraparticle diffusion coefficients of
353 the target adsorbate decrease linearly with d_p (Crittenden et al. 1987; Crittenden et al. 1991),

$$EBCT_{SC} = EBCT_{LC} \cdot \frac{d_{p,SC}}{d_{p,LC}} \quad \text{Eq. (3)}$$

$$HLR_{SC} \geq HLR_{SC,min} = HLR_{LC} \cdot \frac{d_{p,LC}}{d_{p,SC}} \cdot \frac{Re_{SC,min}}{Re_{LC}} \quad \text{Eq. (4)}$$

354 where SC and LC denote the small and large columns, respectively. $HLR_{SC,min}$ and $Re_{SC,min}$ are
355 minimum values of HLR and Reynolds number that are chosen to ensure that dispersion and film
356 mass transfer do not influence overall adsorbate mass transfer in the RSSCT (SC) more than in the
357 pilot column (LC). Typically, a $Re_{SC,min}$ value between 0.1 and 1 is chosen (Crittenden et al. 1991;
358 Crittenden et al. 2012), depending on head loss limitations and Re·Sc values. For this study a $Re_{SC,min}$
359 value of 0.5 was chosen, smaller than the Re_{LC} values of approximately 0.7 for both BC and AA.
360 RSSCTs could have been designed to resemble the CD-RSSCT in Brunson and Sabatini (2014), but
361 design parameters were chosen to more closely resemble typical full-scale AA adsorbers in terms of
362 EBCT and HLR.
363 RSSCTs were constructed from the same materials as the pilot columns, except the columns
364 were either 9.5 mm ID Nylon tubing (CD-RSSCT) or 4.8 mm ID FEP tubing (PD-RSSCT). These
365 tubing sizes corresponded to ratios of d_{bed} to d_p of approximately 45 and 44, respectively, sufficient
366 to avoid wall effects on mass transfer (Knappe et al. 1999). Water was fed to the RSSCTs from 20 L
367 glass carboys using a small diaphragm pump at a constant flow rate to reach the target operational
368 values in Table 2. Although only an EBCT of 10 minutes is shown in Table 2, a simulated full-scale
369 EBCT of 20 minutes was also tested using the PD-RSSCT to evaluate the effect of EBCT as well as
370 two 10-minute EBCT adsorbers operating in series. Prior to loading the BC or AA into the tubing
371 column on a support layer of glass wool, the BC or AA was degassed for 15 minutes using a glass
372 vacuum filter flask and a vacuum pump. To minimize head loss, a glass wool prefilter was placed
373 just after the pump outlet and replaced regularly. pH adjustment and sampling were the same as the
374 pilot column. RSSCT runs were done in duplicate to establish reproducibility.
375
376 **Bone Char Regeneration**
377 While it is well-established that commercial AA can be regenerated using sodium hydroxide, BC is
378 not widely used or produced. Previously mentioned studies that have regenerated BC have done so
379 using batch tests, not fixed-bed adsorbers (Medellin-Castillo et al. 2007; Yami et al. 2017). Therefore,
380 the BC in this study was tested for regenerative properties using the RSSCT starting with a typical
381 procedure for AA regeneration outlined in Clifford et al. (2011). Deionized water for backwashing
382 and rinsing as well as regenerant solutions were fed countercurrent to the RSSCT column on a bed
383 volume (BV) basis because of higher efficiencies associated with countercurrent compared to
384 cocurrent regeneration (Clifford et al. 2011). During normal adsorber operation, BVs represent the
385 volume of water treated divided by the volume of the adsorbent bed. During adsorber regeneration,
386 BVs represent the volume of backwash water or regenerant solution processed divided by the
387 volume of the fixed adsorbent bed. Using a small peristaltic pump and Norprene tubing at a flow
388 rate of approximately 0.7 to 0.8 mL/min, the following backwash, rinse, and regenerant solutions
389 were sequentially fed: 4 BVs of deionized water, 5 BVs of 250 mM sodium hydroxide, 2 BVs of

390 deionized water, 2 BVs of 200 mM sulfuric acid, and 4 BVs of deionized water. The slower than
391 forward flow rate of 2.0 mL/min (Table 2) was chosen to triple the EBCT of each regeneration step
392 (Clifford et al. 2011). Observed BC bed expansion, or fluidization, during regeneration was
393 approximately 100% of the original fixed-bed. Following regeneration, RSSCTs were run under the
394 original operation parameters to evaluate regeneration effectiveness.
395
396 **Results and Discussion**
397
398 **Adsorbent Characterization**
399 BC SEM images are shown in Figure 1(a) through Figure 1(d) and demonstrate the heterogeneous
400 nature of BC particles in terms of particle porosity, shape, and visible macropores. EDS revealed the
401 composition of the BC surface to consist mainly of oxygen (50%), calcium (18%), carbon (17%),
402 and phosphorus (12%) on an atomic basis, consistent with the expected components of most
403 biochars (i.e., carbon), calcium phosphate, and hydroxyapatite. The remaining 3% consisted of
404 sodium, magnesium, and sputter-deposited gold. AA SEM images are shown in Figure 1(e) and
405 Figure 1(f) and do not reveal a porous structure but a rough external surface morphology. EDS
406 revealed the composition of the AA surface to consist solely of oxygen (59%) and aluminum (40%)
407 on an atomic basis, consistent with aluminum oxide. The remaining ~1% consisted of sputter-
408 deposited gold.
409 Surface area and pore volume results for BC and AA are shown in Table 3 and were
410 evaluated on a relative basis, considering that although both N_2 and CO_2 physisorption were
411 successful, they did not provide equivalent results, consistent with Lehmann and Joseph (2015) and
412 Sigmund et al. (2017). AA surface area was approximately 3 to 4 times greater than BC and
413 possessed approximately 2 to 3 times more pore volume. AA N_2 physisorption surface area and total
414 pore volume compared well with BASF product data sheet values of 380 m^2/g and 0.52 cm^3/g,
415 respectively. BC N_2 physisorption surface area, total pore volume, and average pore diameter
416 compared well with published literature values of 85 to 134 m^2/g, 0.30 to 0.38 cm^3/g, and 8 to 11
417 nm, respectively (Medellin-Castillo et al. 2007; Leyva-Ramos et al. 2010; Brunson and Sabatini 2014;
418 Rojas-Mayorga et al. 2015; Medellin-Castillo et al. 2016; Kearns et al. 2018). Surface area, total pore
419 volume, and average pore diameter also compared well between the different BC and AA particle
420 sizes, confirming crushing the BC and AA did not significantly change physical properties.
421
422 **Pilot Column Tests**
423 BC and AA pilot column breakthrough curves at an EBCT of 10 minutes are shown in Figure 2,
424 with throughput shown in BVs. Error bars every 200 BVs represent the spread of duplicate runs,
425 where interpolated effluent concentrations (C), or effluent concentrations normalized by the influent
426 concentration (C/C_0), were averaged every 50 BVs. AA outperformed BC for the entire
427 breakthrough curve, but within the first 350 BVs, both BC and AA removed fluoride to below 0.1
428 mg/L. Fluoride in BC effluent reached the WHO guideline or treatment objective concentration
429 (C_{TO}) of 1.5 mg/L after approximately 450 BVs or 3.1 days, while fluoride in AA effluent reached
430 C_{TO} after approximately 650 BVs or 4.5 days. The breakthrough curves in Figure 2 show AA treated
431 approximately 44% more water than BC prior to reaching C_{TO}. Within approximately 2,000 BVs, BC
432 reached near exhaustion at 85 to 90% breakthrough while AA plateaued near 50 to 70% from
433 approximately 1,100 to 2,000 BVs. The AA breakthrough behavior may have been a result of
434 increased mass transfer resistance due to increased stagnant film thickness surrounding AA particles
435 from operating at a low HLR, but typical HLR operating conditions also exhibit mass transfer
436 limitations and do not allow for full utilization of AA fluoride adsorption capacity (Clifford et al.
437 2011, EPA 2014).

438 Although complete AA-fluoride breakthrough curves, like the one shown in Figure 2 are
439 limited in published literature (Clifford et al. 1991, 2011), breakthrough to C_{TO} agrees well with
440 previous studies under similar conditions (C_0: 5.0-10.8 mg/L, pH 5.5-6.6), with C_{TO} occurring
441 between approximately 500 and 1,200 BVs (Clifford et al. 2011; EPA 2014). For BC, complete
442 fluoride breakthrough curves like the one shown in Figure 2 are also limited in published literature
443 (Brunson and Sabatini 2014; Yami et al. 2017; Kearns et al. 2018), especially with d_p values close to
444 0.92 mm. Brunson and Sabatini (2014) and Yami et al. (2017) generated BC-fluoride breakthrough
445 curves using d_p values of 0.64 and 0.4 mm. Their BC columns reached C_{TO} at approximately 100 and
446 350 BVs with fluoride C_0 values of 8.6 and 9.2 mg/L, respectively, indicating less adsorption
447 capacity than the BC used in this study. Testing a groundwater with a similar fluoride C_0 of 8.5
448 mg/L and an unadjusted pH of 8.2, Kearns et al. (2018) observed breakthrough to C_{TO} at
449 approximately 250 BVs using an EBCT of 38 minutes and d_p of 1.3 mm. Kearns et al. (2018) likely
450 observed earlier breakthrough compared to Figure 2 due to the high influent pH.
451 Considering the bed densities (ρ_{bed}) for BC and AA were different as shown in Table 2,
452 breakthrough curves were also compared using specific throughput (ST) or the amount of water
453 treated divided by the mass of adsorber bed ($ST = {BV}/{\rho_{bed}}$) and the inverse of ST, which is the
454 adsorbent UR prior to regeneration. Using ρ_{bed} values from Table 2 of 630 and 560 g/L for BC and
455 AA, respectively, ST values at C_{TO} for BC and AA were 0.7 and 1.2 L/g. Therefore, on a ST basis,
456 AA treated approximately 71% more water per mass of adsorbent. Corresponding UR values for BC
457 and AA were 1.4 and 0.9 g/L, respectively. Therefore, on an UR basis, AA required approximately
458 36% less adsorbent to treat the same amount of water. Although both AA and BC can be
459 regenerated, URs can be thought of as one-time adsorbent doses to a batch reactor and illustrate the
460 quantity of both BC and AA required to remove fluoride from solution.
461 Solid phase concentrations (q) were also estimated from integrating above the breakthrough
462 curves in Figure 2 using Eq. (5),

$$q = \frac{C_0}{\rho_{bed}} \sum_{i=2}^{n} \left(1 - \frac{C_i}{C_0}\right)(BV_i - BV_{i-1}) \qquad \text{Eq. (5)}$$

463 where BV_1=0. At C_i=C_{TO}, q values were 5.8 and 9.4 mg fluoride per g of adsorbent (mg/g) for BC
464 and AA, respectively. If q values are normalized by the N_2 surface area values from Table 3, BC
465 exhibited higher fluoride adsorption per unit area compared to AA, where the surface fluoride
466 concentrations were 0.070 and 0.027 mg/m^2 of adsorbent, respectively. These results indicate BC
467 has a higher affinity for fluoride (i.e., higher adsorption site density) compared with AA and that
468 higher pyrolysis temperatures may be necessary to maximize BC surface area and resulting fluoride
469 adsorption. Using Eq. (5), q values of 12 and 19 mg/g were calculated for BC and AA. Running
470 each adsorbent to C_{TO} used approximately 50% of the total adsorption capacity identified in this
471 study, highlighting the benefit of running adsorbers in series, discussed in subsequent sections.
472 As a comparison, literature q values for BC and fluoride in equilibrium batch studies, using
473 either Freundlich or Langmuir isotherm equation-fitting, range from approximately 2 to 16 mg/g
474 under varying conditions of pH, BC surface modifications, and equilibrium fluoride concentrations
475 (Medellin-Castillo et al. 2007; Brunson and Sabatini 2014; Medellin-Castillo et al. 2016; Yami et al.
476 2017). Therefore, q values in this study evaluated to an effluent value of C_{TO} and over the entire
477 breakthrough curve fall within expected values of batch studies and were generated concomitantly
478 with operational information.
479
480 **Rapid Small-Scale Column Tests with Bone Char**

481 BC pilot column, CD-RSSCT, and PD-RSSCT breakthrough curves are shown in Figure 3, where
482 error bars and averaging duplicate runs were applied using the same method as the pilot column. In
483 terms of adsorption capacity, neither the CD-RSSCT nor the PD-RSSCT was able to adequately
484 predict the pilot column over the entire breakthrough, with both showing overall less adsorption
485 capacity for fluoride. The CD-RSSCT exhibited almost immediate breakthrough, indicating the
486 length of the mass transfer zone was approximately the column length of 3.8 cm (Table 2). Using
487 Eq. (5), the CD-RSSCT breakthrough curve yielded a q value of 6.3 mg/g, or 53% of the pilot
488 column q value of 12 mg/g, while the PD-RSSCT breakthrough curve yielded a q value of 6.9 mg/g,
489 or 58% of the pilot column q value of 12 mg/g. Relative to each other, CD-RSSCT and PD-RSSCT
490 q values confirmed the assumption that adsorption capacity does not significantly change with BC
491 particle size. Similar isotherm adsorption capacities, with smaller BC particles exhibiting slightly
492 more capacity, were also observed by Leyva-Ramos et al. (2010) for three different BC particle sizes.
493 However, this assumption did not hold in this study for larger differences in particle size, as the
494 smaller particle size in the RSSCTs exhibited considerably less overall fluoride adsorption capacity
495 than the pilot column.
496 Short duration batch experiments were performed to evaluate the differences, if any, in
497 adsorption capacity as a function of d_p. Approximately 50 mg of each size BC was added to 50 mL
498 of raw groundwater (1.0 g/L dose) and mixed using a stir bar and plate for 48 hours, run in
499 duplicates. Solid phase loadings were similar to the findings of Levya et al. (2010), in that although
500 the small particles exhibited slightly more capacity (100x200 BC: 2.4±0.4 mg/g, 60x80 BC: 2.1±0.3
501 mg/g) than the large particles (12x40 BC: 1.9±0.3 mg/g), the group means were not statistically
502 significant at the 95% confidence level using Tukey's Method ($p=0.446$). Considering these results
503 and the physical properties of the different BC particles sizes were similar (Table 3), it is unknown
504 why the smaller particle sizes exhibited less adsorption capacity in the RSSCTs. As previously stated,
505 the RSSCT typically uses matching pilot column studies to provide accurate predictions, and this
506 work establishes that requirement for this specific water and adsorbent combination.
507 Nevertheless, one hypothesis to explain RSSCT and pilot results is the adsorption of fluoride
508 was not instantaneous (i.e., local equilibrium) as others have assumed (Leyva-Ramos et al. 2010). A
509 fast adsorption step is generally assumed for physical adsorption of organic constituents to GAC
510 while chemical adsorption may increase the time for adsorption to occur (Summers et al. 2011). In
511 addition to diffusional mass transfer resistances and the assumption that the actual adsorption to the
512 BC surface should be independent of particle size, the $EBCT_{SC}$ values of 0.5 and 1.2 minutes (and
513 the longer $EBCT_{SC}$ value of 2.4 minutes discussed in subsequent sections), could have been
514 insufficient for sustained fluoride removal as observed in the pilot column. By comparison, the
515 $EBCT_{LC}$ and $EBCT_{SC}$ values tested by Brunson and Sabatini (2014) were considerably longer at 29
516 and 6.6 minutes, respectively. Pilot columns and RSSCTs with longer EBCTs could be tested to
517 further investigate whether the adsorption rate contributes to decreasing apparent fluoride
518 adsorption capacity with decreasing BC particle size.
519 While adsorption capacity governs the extent of or area above breakthrough curves,
520 adsorption kinetics, or film and intraparticle diffusion mass transfer resistances, govern the shape
521 (e.g., sharpness) of adsorption breakthrough curves. Isotherm parameters such as the Freundlich
522 1/n values also influence the shape of breakthrough curves but are not discussed herein. In Figure 3,
523 the shape of CD-RSSCT breakthrough curve matches well with the pilot column, indicating
524 intraparticle diffusion coefficients (D_s and D_p) were similar across different the two BC particle sizes
525 and film mass transfer was important. In general, the CD-RSSCT results indicate intraparticle
526 diffusion coefficients of fluoride within BC pores is independent of BC particle size, consistent with
527 the findings of Leyva et al. (2010) and Brunson and Sabatini (2014). This response was not observed
528 for the PD-RSSCT, which showed much faster adsorption kinetics through a steeper breakthrough

529 curve compared to the CD-RSSCT breakthrough curve. This result was expected considering film
530 mass transfer resistance is inherently reduced in the PD design (Eq. (4)). While intraparticle diffusion
531 typically controls mass transfer resistance for adsorbents that have higher internal than external
532 surface area (Crittenden et al. 1991; Westerhoff et al. 2005; Leyva-Ramos et al. 2010; Nigri et al.
533 2017), film mass transfer may have been more important than this PD design allowed.
534 Despite differences in overall adsorption capacity and the CD-RSSCT's apparent simulation
535 of adsorption kinetics, for practical purposes the PD-RSSCT breakthrough curve in Figure 3
536 provided an adequate and conservative prediction of the BC pilot column breakthrough up to and
537 slightly beyond C_{TO}. Therefore, for preliminary evaluations of potential full-scale BC absorbers, the
538 PD-RSSCT may provide more useful predictions of fluoride breakthrough and related operational
539 parameters. Additionally, as shown in Table 2, the PD-RSSCT required the least amount of
540 groundwater, less than 3 L, to generate breakthrough curves in less than one day. It should not be
541 discounted the CD-RSSCT may still provide useful evaluations of fluoride adsorption to BC and did
542 yield a successful prediction between two different BC particle sizes (Brunson and Sabatini 2014).
543
544 **Rapid Small-Scale Column Tests with Activated Alumina**
545 AA pilot column, CD-RSSCT, and PD-RSSCT breakthrough curves are shown in Figure 4, where
546 error bars and averaging from duplicate runs were applied using the same method as the pilot
547 column. Comparing BC trends shown in Figure 3 with AA trends in Figure 4, similarities in fluoride
548 mass transfer exist between the two materials despite different physical/chemical properties and
549 adsorption capacities. Again, neither the CD-RSSCT nor the PD-RSSCT was able to adequately
550 predict the pilot column over the entire breakthrough, with both showing overall less adsorption
551 capacity for fluoride. Using Eq. (5), the CD-RSSCT breakthrough curve yielded a q value of 14
552 mg/g, or 74% of the pilot column q value of 19 mg/g, while the PD-RSSCT breakthrough curve
553 yielded a q value of 13 mg/g, or 68% of the pilot column q value of 19 mg/g.
554 The same short duration batch tests as BC were performed with each size AA and yielded
555 similar results, in that all exhibited comparable adsorption capacities (100x200 AA: 1.3±0.1 mg/g,
556 60x80 AA: 1.2±0.1 mg/g, 16x30 AA: 1.4±0.2 mg/g) where the group means were not statistically
557 significant at the 95% confidence level using Tukey's Method ($p=0.493$). Surprisingly, the BC
558 exhibited more capacity than AA during batch testing, which merits further investigation. Therefore,
559 the same hypothesis is put forth, in that similar to BC, AA $EBCT_{SC}$ values of 0.6 and 1.3 minutes
560 (and the longer $EBCT_{SC}$ value of 2.6 minutes discussed in subsequent sections) could have been
561 insufficient for the sustained fluoride removal observed in the pilot column. In other words, the
562 adsorption rate of fluoride to the AA surface may have been important in addition to diffusional
563 mass transfer resistances. Like BC, it appears that fluoride adsorption kinetics for AA were better
564 simulated using the CD-RSSCT (i.e., similar breakthrough curve shapes).
565 Although not as good of a prediction compared to BC, the PD-RSSCT provided an
566 adequate and conservative prediction of the AA pilot column up to and slightly beyond C_{TO}. As
567 shown in Table 2, this experiment required less than 4 L of water to generate breakthrough curves in
568 less than two days. For preliminary evaluations of potential full-scale AA absorbers, the PD-RSSCT
569 may provide more adequate and useful predictions of fluoride breakthrough to C_{TO} and related
570 operational parameters. Conveniently, comparisons between BC and AA can then be simplified
571 through use of the same RSSCT design.
572
573 **Empty Bed Contact Time and Adsorbers in Series**
574 A major benefit of the RSSCT over batch studies is the direct evaluation of specific design criteria,
575 specifically EBCT, and determining optimal adsorber configuration (series or parallel). EBCT is one
576 of the most important design parameters for adsorption processes as it impacts both capital and

577 operational costs (i.e., regeneration frequency) of adsorber systems. The PD-RSSCT was identified
578 as the RSSCT design of most practical use because it provided better predictions of full-scale
579 fluoride breakthrough for both BC and AA comparing pilot column and RSSCT breakthrough
580 curves (Figure 3 and Figure 4). Therefore, the PD-RSSCT was used to compare full-scale EBCTs of
581 10 and 20 minutes for both BC and AA in addition to operation of adsorbers in series. Not shown
582 in Table 2, the longer $EBCT_{SC}$ values were 2.4 and 2.6 minutes for BC and AA, respectively. While
583 both series and parallel operation can improve URs, only series operation was tested because it is
584 more typical for AA (Clifford et al. 2011; EPA 2014) and is better suited to higher levels of removal
585 (C/C_0=0.18 in this case) (Summers et al. 2011; Crittenden et al. 2012). In prior work series operation
586 has also been shown to yield more favorable BC URs compared to parallel operation (Kearns et al.
587 2018).
588 BC and AA breakthrough curves on a throughput basis at the two EBCTs are shown Figure
589 5a. Since the 10- and 20-minute breakthrough curves are nearly indistinguishable for both BC and
590 AA, it can be concluded in this case that doubling the EBCT, or size of the adsorber, provided a
591 minimal increase in ST or decrease in adsorbent UR to C_{TO}. Doubling the amount of adsorbent did
592 not increase fluoride removal efficiency as the fluoride mass transfer zone was less than the 10-
593 minute EBCT, hence validating the industry standard EBCT of 5 minutes for AA. Although not
594 tested in this study, the PD-RSSCT could be used to determine if a more optimal EBCT exists for
595 both BC and AA in addition to providing preliminary estimations of capital and operational costs.
596 BC and AA breakthrough curves on a time basis as two 10-minute EBCT adsorbers in
597 series, or lead-lag operation, are shown in Figure 5b. The lead BC adsorber run would reach C_{TO}
598 after approximately 2.5 days, corresponding to a UR of 1.9 g/L. PD-RSSCT breakthrough curves as
599 a function of time demonstrate increased UR compared to a single adsorber as the lead adsorber can
600 be operated until either the lag adsorber reaches C_{TO} or the lead adsorber is fully exhausted. Under
601 these test conditions with two adsorbers in series, the lead and lag adsorber could run until the lag
602 adsorber reaches C_{TO} at approximately 5.5 days, a UR of 1.3 g/L (32% reduction), estimated using
603 Eq. (6) (Crittenden et al. 2012),

$$UR = \left(\frac{q_{lead}}{C_0} + \frac{C_{TO}\Delta t_{lag}}{2C_0 EBCT_{lag}\rho_{bed}}\right)^{-1} \qquad \text{Eq. (6)}$$

604 where q_{lead} is the solid phase loading on the lead adsorber (estimated using Eq. (5)), $EBCT_{lag}$ is the
605 EBCT of the lag adsorber (10 minutes), Δt_{lag} is the time from incipient breakthrough to C_{TO} for the
606 lag adsorber (~1.5 days from Figure 5b), and all other terms have been previously defined. A similar
607 BC UR reduction of 46% through series operation was realized by Kearns et al. (2018). The same
608 analysis for AA yielded a single adsorber UR of 1.2 g/L and a two adsorbers in series UR of 0.7 g/L,
609 a 42% UR reduction, corresponding to an AA lead adsorber runtime increase from 3.5 to 7.5 days.
610
611 **Bone Char Regeneration**
612 Fresh and regenerated BC breakthrough curves using the PD-RSSCT are shown in Figure 6a. Using
613 BVs to C_{TO} as an estimate for q, the first three runs following regeneration exhibited an
614 approximately 50% reduction in adsorption capacity compared to fresh BC (C_{TO} at ~300 BVs).
615 Approximately the same adsorption capacity was observed comparing the subsequent runs to each
616 other (C_{TO} at ~150 to 200 BVs). These results indicate that the regeneration was incomplete likely
617 due to (1) insufficient concentration or BVs of sodium hydroxide regenerant solution, (2) channeling
618 and short circuiting impacting how the sodium hydroxide regenerant solution was hydraulically
619 contacting BC in the column, and/or (3) permanent reductions in BC capacity for fluoride due to
620 competitive adsorption.

621 To evaluate the impact of regenerant exposure, fluoride regeneration elution curves were
622 generated during the 3rd and 4th regeneration cycles and are shown in Figure 6b. During the 3rd
623 regeneration, 5 BVs of 250 mM sodium hydroxide regenerant were applied while during the 4th
624 regeneration 43 BVs were excessively applied to be conservative. Significantly more fluoride was
625 eluted during the 4th regeneration compared to the 3rd, approximately 7.2 mg compared to 2.8 mg,
626 confirming the first three regenerations were incomplete from inefficient exposure to the regenerant.
627 The limited leakage of fluoride following the regeneration cycles indicated that fluoride had likely
628 been completely regenerated and rinsed from the lower bed of the PD-RSSCT shown in Fig 6a. The
629 gradual decrease of eluted fluoride in the 4th regeneration elution curve shown in Figure 6b is
630 indicative of non-uniform BC exposure to the regenerant solution. A reason for the gradual decrease
631 of fluoride or tailing effect is from BC particles moving within the PD-RSSCT bed while
632 inefficiently being contacted with the regenerant solution. In this study BC was fluidized during the
633 countercurrent regeneration, however, to ensure uniform regenerant exposure it is prudent to
634 maintain a fixed-bed. Similar regeneration processes employed for ion exchange use blocking
635 air/water or inert material to maintain the bed fixed during a countercurrent regeneration. Future
636 research could implement the PD-RSSCT to investigate BC regeneration configurations and
637 methods.
638 Aside from potential regenerant exposure deficiencies, it is known arsenic competes for
639 adsorption sites on both BC and AA when in the arsenate ($H_2AsO_4^-$) form (Sorg 1978; Clifford et al.
640 1991; Mlilo et al. 2010), and arsenic adsorption to BC may be irreversible (Sorg 1978). Raw
641 groundwater was not initially sampled for arsenic, but due to regeneration trends observed in Fig 6a,
642 raw groundwater from two different sample dates was analyzed for total arsenic according to EPA
643 Method 200.8. Analysis revealed an average arsenic concentration of 0.022±0.001 mg/L,
644 approximately twice the EPA MCL of 0.010 mg/L. Therefore, in addition to inefficient exposure to
645 the regenerant solution, the BC adsorption capacity for fluoride may have been permanently reduced
646 by irreversible arsenic adsorption. Dissolved organic matter (DOM), as measured by DOC and
647 UVA_{254} (Table 1) may also have permanently reduced BC adsorption capacity considering the high
648 specific UVA_{254} ($SUVA_{254}=UVA_{254}\cdot 100/DOC$) value of 3.7 (Edzwald and Tobiason 2011), but this
649 was not expected as groundwater DOM is generally weakly adsorbed and previous batch studies did
650 not show significant DOM competition (Brunson and Sabatini 2014). Further BC studies are
651 recommended to quantify the extent of competitive adsorption and capacity reductions from arsenic
652 and DOM.
653
654 **Conclusion**
655 Using groundwater containing relatively high levels of naturally-occurring fluoride (8.5 mg/L), BC
656 and AA were compared using the fixed-bed adsorbers of pilot columns, CD-RSSCTs, and PD-
657 RSSCTs. AA outperformed BC breakthrough curves by approximately 200 BVs or 1.5 days to C_{TO}
658 of 1.5 mg/L reinforcing why it is considered the best available technology. However, per m^2 of
659 adsorbent surface area, fluoride concentrations were higher on the BC compared to AA, indicating
660 that maximizing BC surface area may improve adsorption capacity. CD-RSSCTs and PD-RSSCTs
661 demonstrated that fluoride breakthrough curves could be generated in less time and requiring less
662 water compared to pilot columns. Although the CD-RSSCT appeared to provide a better simulation
663 of adsorption kinetics, as determined by the shape of the breakthrough curve, the PD-RSSCT
664 provided better predictions of both BC and AA pilot column breakthrough to reaching C_{TO}. As
665 such, the PD-RSSCT was used to demonstrate that increasing the full-scale EBCT from 10 to 20
666 minutes for both BC and AA did not result in better URs. The same data set was used to
667 demonstrate running BC and AA adsorbers in series results in higher URs and longer adsorber
668 runtimes. The PD-RSSCT and sodium hydroxide were used to regenerate BC and produce several

post-regeneration breakthrough curves. During subsequent treatment and regeneration cycles, earlier fluoride breakthrough compared to fresh BC was observed. Coupled with additional water quality analysis on the raw groundwater, it was determined that insufficient exposure to the regenerant solution and the presence of arsenic likely reduced the BC adsorption capacity for fluoride.

References

Abe, I., Iwasaki, S., Tokimoto, T., Kawasaki, N., Nakamura, T., and Tanada, S. (2004). "Adsorption of fluoride ions onto carbonaceous materials." *J. Colloid Interface Sci.*, 274(1), 35-39.

Amini, M., Mueller, K., Abbaspour, K.C., Rosenberg, T., Afyuni, M., Moller, K.N., Sarr, M., and Johnson, C.A. (2008). "Statistical modeling of global geogenic fluoride contamination in groundwaters." *Environ. Sci. Tech.*, 42(10), 3662-3668.

Ayoob, S., Gupta, A.K., and Bhat, V.T. (2008). "A conceptual overview on sustainable technologies for the defluoridation of drinking water." *Crit. Rev. Environ. Sci. Technol.*, 38(6), 401-470.

Brunson, L.R., and Sabatini, D.A. (2014). "Practical considerations, column studies and natural organic material competition for fluoride removal with bone char and aluminum amended materials in the Main Ethiopian Rift Valley." *Sci. Total Environ.*, 488-489, 580-587.

Clifford, D., Lin, C.C., and Sorg, T.J. (1991). Arsenic(III) and arsenic(V) removal from drinking water in San Ysidro, New Mexico (EPA/600/2-91/011). United States Environmental Protection Agency, Drinking Water Research Division, Risk Reduction Engineering Laboratory, Cincinnati, OH.

Clifford, D., Sorg, T.J., and Ghurye, G.L. (2011). "Ion Exchange and Adsorption of Inorganic Contaminants." Chapter 12 in *Water Quality & Treatment: A Handbook on Drinking Water*, 6th edition, American Water Works Association, Denver, CO.

Corwin, C.J., and Summers, R.S. (2010). "Scaling trace organic contaminant adsorption capacity by granular activated carbon." *Environ. Sci. Technol.*, 44(14), 5403-5408.

Crittenden, J.C., Berrigan, J.K., and Hand, D.W. (1986a). "Design of rapid small-scale adsorption tests for a constant diffusivity." *J. Water Pollut. Control Fed.*, 58(4), 312-319.

Crittenden, J.C., Hutzler, N.J., Geyer, D.G., Oravitz, J.L., and Friedman, G. (1986b). "Transport of organic compounds with saturated groundwater flow: model development and parameter sensitivity." *Water Resour. Res.*, 22(3), 271-284.

Crittenden, J.C., Berrigan, J.K., Hand, D.W., and Lykins, B. (1987). "Design of rapid fixed-bed adsorption tests for nonconstant diffusivities." *J. Environ. Eng.*, 113(2), 243-259.

Crittenden, J.C., Reddy, P.S., Arora, H., Trynoski, J., Hand, D.W., Perram, D.L., and Summers, R.S. (1991). "Predicting GAC performance with rapid small-scale column tests." *J. Am. Water Works Assoc.*, 83(1), 77-87.

Crittenden, J.C., Trussell, R.R., Hand, D.W., Howe, K.J., and Tchobanoglous, G. (2012). "Adsorption." Chapter 15 in *Water Treatment – Principles and Design*, 3rd edition, John Wiley & Sons, Inc., Hoboken, NJ.

Edzwald, J.K., and Tobiason, J.E. (2011). "Chemical Principles, Source Water Composition, and Watershed Protection." Chapter 3 in *Water Quality & Treatment: A Handbook on Drinking Water*, 6th edition, American Water Works Association, Denver, CO.

EPA (2014). "Design Manual – Removal of Fluoride from Drinking Water Supplies by Activated Alumina." Prepared by ALSA Tech, LLC, North Bethesda, MD and Battelle, Columbus, OH, for United States Environmental Protection Agency, Water Supply and Water Resources Division, Cincinnati, OH.

Fan, X., Parker, D.J., and Smith, M.D. (2003). "Adsorption kinetics of fluoride on low cost materials." *Water Res.*, 37(20), 4929-4937.

Fawell, J., Bailey, K., Chilton, J., Dahi, E., Fewtrell, L., and Magara, Y. (2006). "Fluoride in Drinking-water." Published on behalf of the World Health Organization, IWA Publishing, London, United Kingdom.

Haynes, W.M., Lide, D.R., and Bruno, T.J. (2016). "CRC Handbook of Chemistry and Physics." 97th edition, CRC Press, Taylor & Francis Group, Boca Raton, FL.

Hao, O.J., and Huang, C.P. (1986). "Adsorption characteristics of fluoride onto hydrous alumina." *J. Environ. Eng.*, 112(6), 1054-1069.

Kaprara, E., Tziarou, N., Kalaitzidou, K., Simeonidis, K., Balcells, L., Pannunzio, E.V., Zouboulis, A., and Mitrakas, M. (2017). "The use of Sn(II) oxy-hydroxides for the effective removal of Cr(VI) from water: Optimization of synthesis parameters." *Sci. Total Environ.*, 605-606, 190-198.

Kearns, J., Krupp, A., Diek, E., Mitchell, S., Dossi, S., and Hartman, S. (2018). "Lead-lag series and staged parallel operational strategies improve the performance and cost-effectiveness of bonechar for control of fluoride in groundwater." *J. Water. Sanit. Hyg. Dev.*, 8(4), 777-784.

Kennedy, A.M., Reinert, A.M., Knappe, D.R.U., and Summers, R.S. (2017). "Prediction of full-scale GAC adsorption of organic micropollutants." *Environ. Eng. Sci.*, 34(7), 496-507.

Knappe, D.R.U., Snoeyink, V.L., Roche, P., Prados, M.J., and Bourbigot, M.M. (1999). "Atrazine removal by preloaded GAC." *J. Am. Water Works Assoc.*, 91(10), 97-109.

Lehmann, J., and Joseph, S. (2015). "Biochar for Environmental Management: Science, Technology and Implementation." 2nd edition, Routledge, New York, NY.

Leyva-Ramos, R., Rivera-Utrilla, J., Medellin-Castillo, N.A., and Sanchez-Polo, M. (2010). "Kinetic modeling of fluoride adsorption from aqueous solution onto bone char." *Chem. Eng. J.*, 158(3), 458-467.

Medellin-Castillo, N.A., Leyva-Ramos, R., Ocampo-Perez, R., Garcia de la Cruz, R.F., Aragon-Pina, A., Martinez-Rosales, J.M., Guerrero-Coronado, R.M., and Fuentes-Rubio, L. (2007). "Adsorption of fluoride from water solution on bone char." *Ind. Eng. Chem. Res.*, 46(26), 9205-9212.

Medellin-Castillo, N.A., Padilla-Ortega, E., Tovar-Garcia, L.D., Leyva-Ramos, R., Ocampo-Perez, R., Carrasco-Marin, F., and Berber-Mendoza, M.S. (2016). "Removal of fluoride from aqueous solution using acid and thermally treated bone char." *Adsorption*, 22(7), 951-961.

Mlilo, T.B., Brunson, L.R., and Sabatini, D.A. (2010). "Arsenic and Fluoride Removal Using Simple Materials." *J. Environ. Eng.*, 136(4), 391-398.

Nigri, E.M., Cechinel, M.A.P., Mayer, D.A., Mazur, L.P., Loureiro, J.M., Rocha, S.D.F., and Vilar, V.J.P. (2017). "Cow bones char as a green sorbent for fluorides removal from aqueous solutions: batch and fixed-bed studies." *Environ. Sci. Pollut. Res.*, 24(3), 2364-2380.

NRC. (2006). "Fluoride in Drinking Water – A Scientific Review of EPA's Standards." National Research Council of the National Academies, The National Academies Press, Washington, DC.
PHS. (2015). "US Public Health Service recommendation for fluoride concentration in drinking water for the prevention of dental caries." *Public Health Rep.*, 130(4), 318-331.

Rojas-Mayorga, C.K., Bonilla-Petriciolet, A., Sanchez-Ruiz, F.J., Moreno-Perez, J., Reynel-Avila, H.E., Aguayo-Villarreal, I.A., and Mendoza-Castillo, D.I. (2015). "Breakthrough curve modeling of liquid-phase adsorption of fluoride ions on aluminum-doped bone char using micro-columns: effectiveness of data fitting approaches." *J. Mol. Liq.*, 208, 114-121.

Sigmund, G., Huffer, T., Hofmann, T., and Kah, M. (2017). "Biochar total surface area and total pore volume determined by N_2 and CO_2 physisorption are strongly influenced by degassing temperature." *Sci. Total Environ.*, 580, 770-775.

Sorg, T.J. (1978). "Treatment technology to meet the interim primary drinking water regulations for inorganics." *J. Am. Water Works Assoc.*, 70(2), 105-112.

Summers, R.S., Knappe, D.R.U, and Snoeyink, V.L. (2011). "Adsorption of Organic Compounds by Activated Carbon." Chapter 14 in *Water Quality & Treatment: A Handbook on Drinking Water*, American Water Works Association, Denver, CO.

Westerhoff, P., Highfield, D., Badruzzaman, M., and Yoon, Y. (2005). "Rapid small-scale column tests for arsenate removal in iron oxide packed bed columns." *J. Environ. Eng.*, 131(2), 262-271.
WHO. (2017). "Guidelines for Drinking Water Quality." 4th edition, World Health Organization, Geneva, Switzerland.

Yami, T.L., Chamberlain, J.F., Butler, E.C., and Sabatini, D.A. (2017). "Using a high-capacity chemically activated cow bone to remove fluoride: field-scale column tests and laboratory regeneration studies." *J. Environ. Eng.*, 143(2), 04016083, 1-9.

Figures

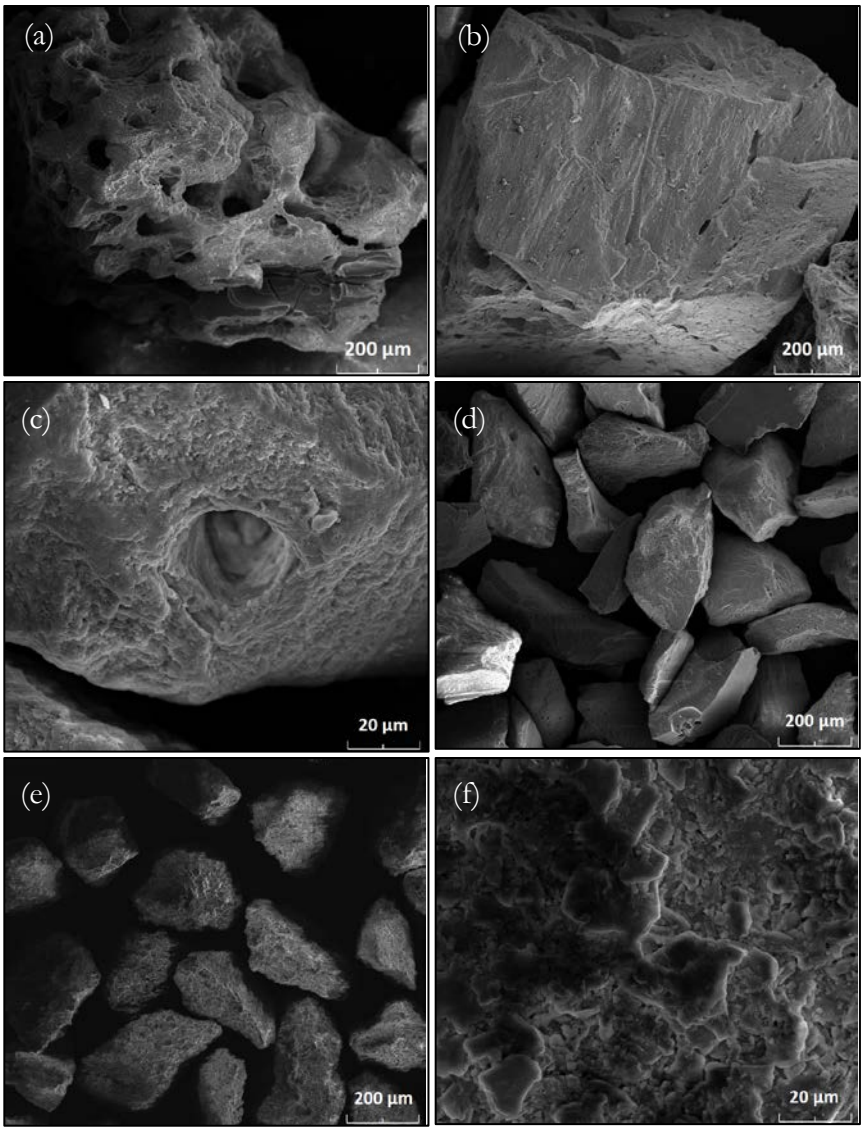

Figure 1. SEM images of (a) and (b) BC (dp=0.92 mm), (c) and (d) BC (dp=0.21 mm), (e) and (f) AA (dp=0.21 mm).

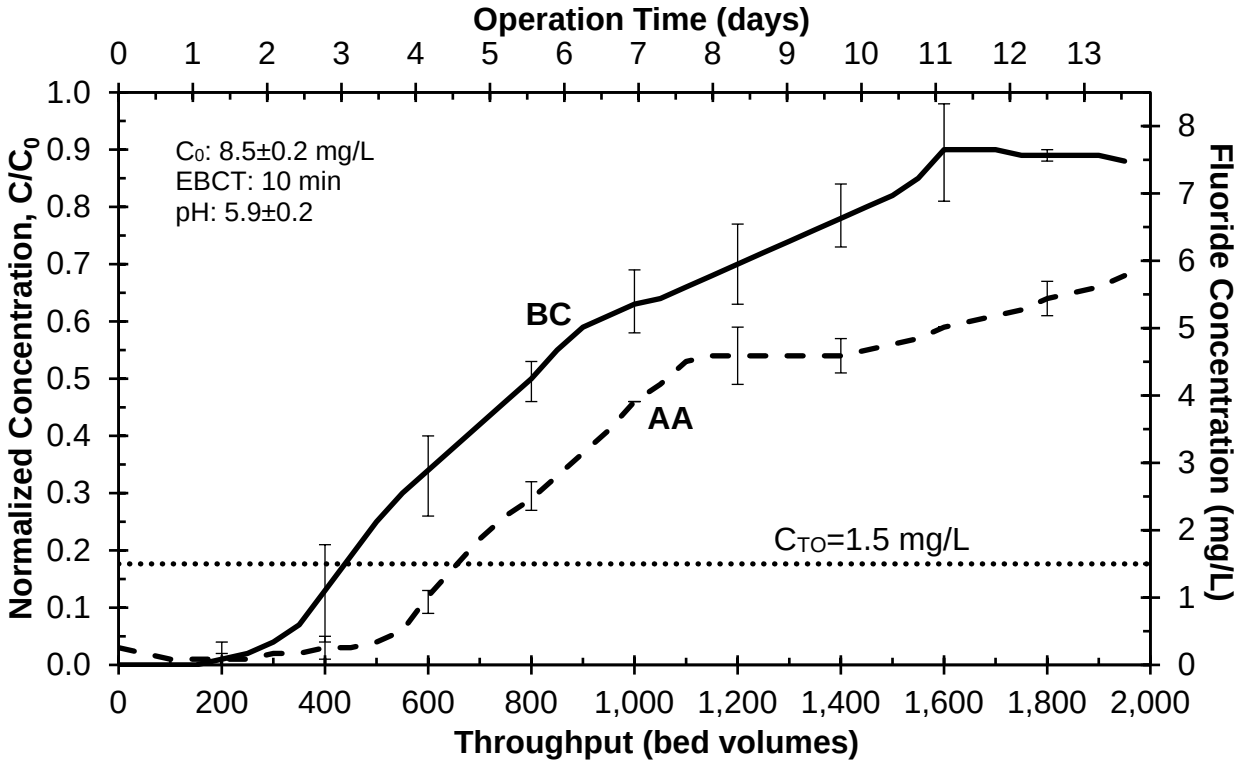

Figure 2. Pilot column fluoride breakthrough curves for BC (dp=0.92 mm) and AA (dp=0.86 mm). Error bars represent the spread of duplicate runs.

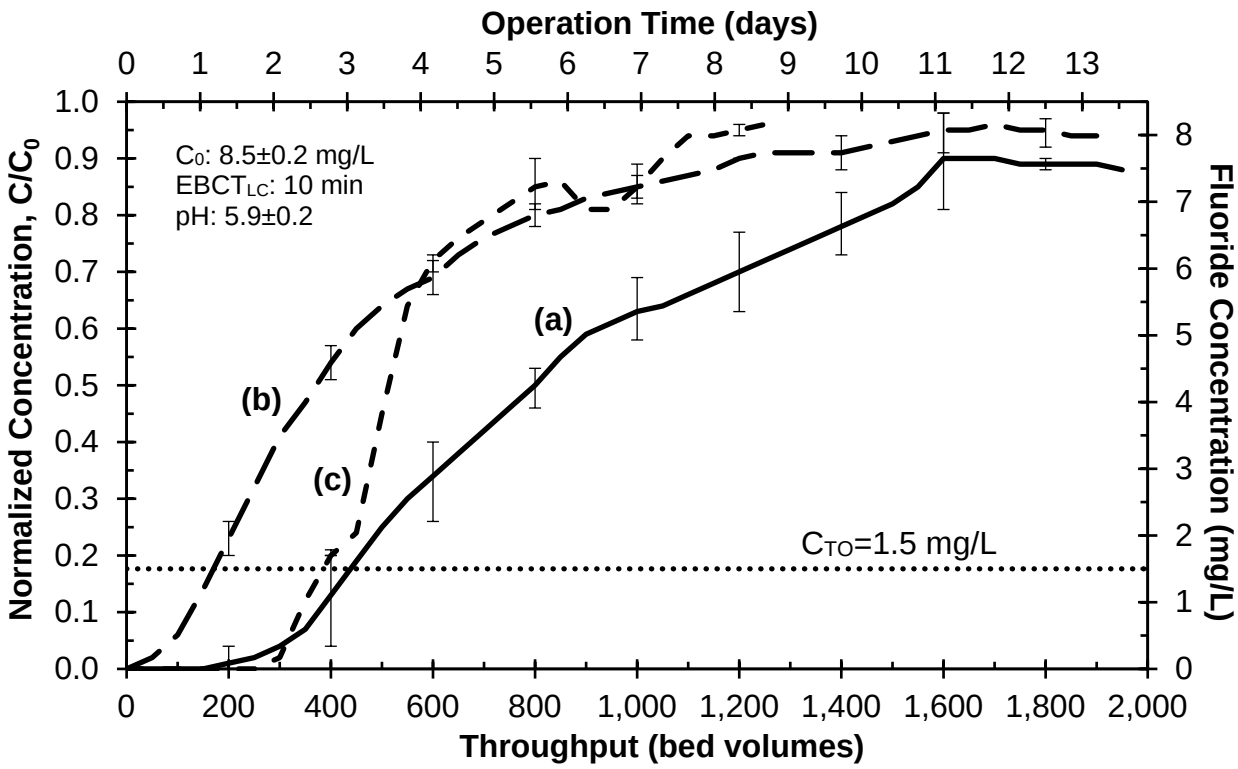

Figure 3. Fluoride breakthrough curves for BC (a) pilot column (dp=0.92 mm), (b) CD-RSSCT (dp=0.21 mm), and (c) PD-RSSCT (dp=0.11 mm). Error bars represent the spread of duplicate runs.

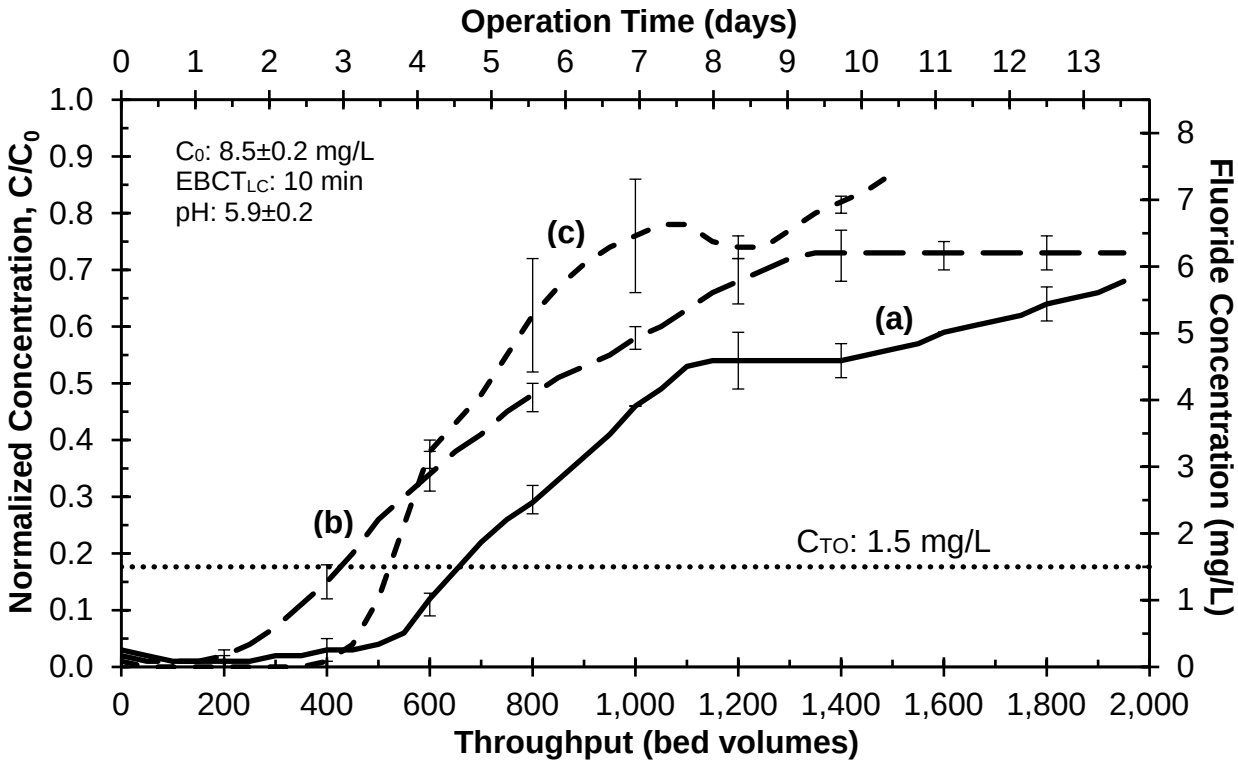

Figure 4. Fluoride breakthrough curves for AA (a) pilot column (dp=0.86 mm), (b) CD-RSSCT (dp=0.21 mm), and (c) PD-RSSCT (dp=0.11 mm). Error bars represent the spread of duplicate runs.

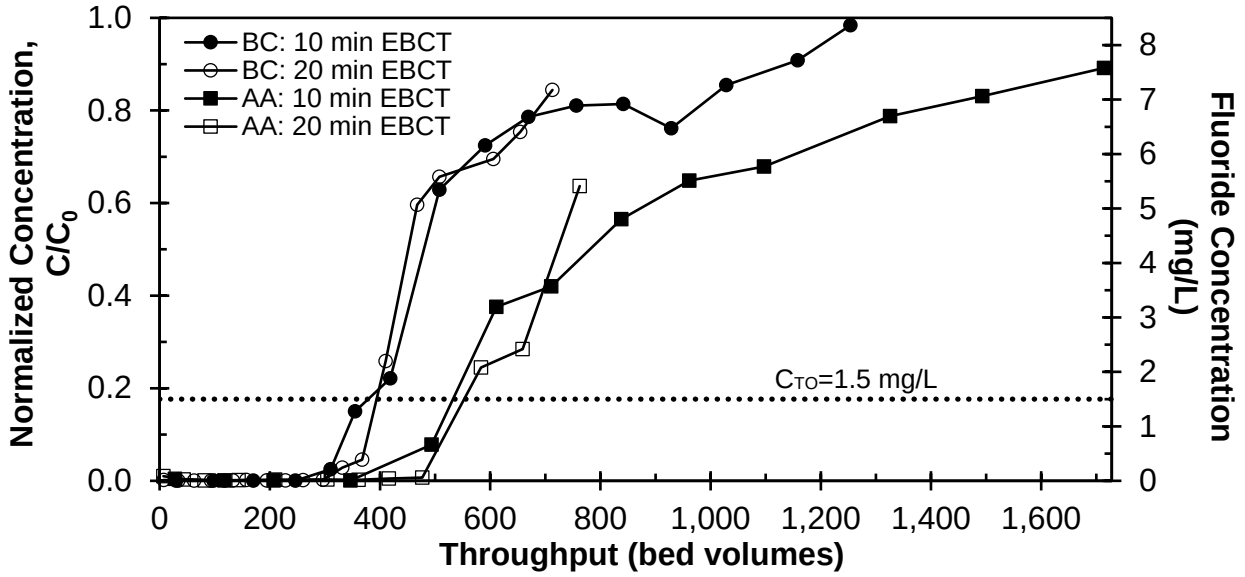

(a)

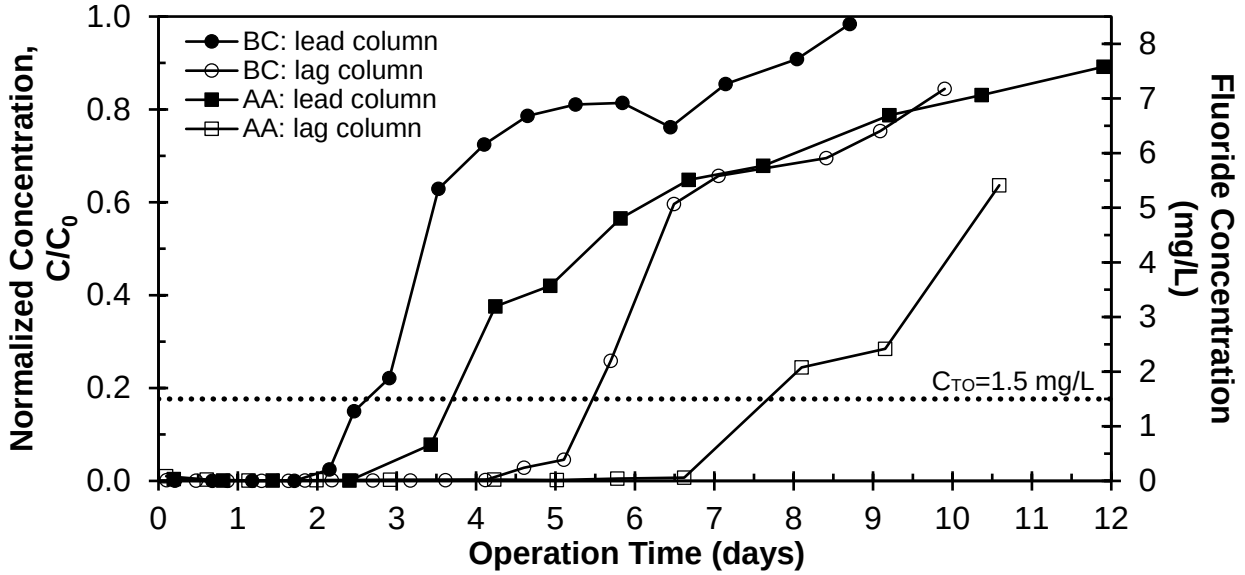

(b)

Figure 5. Fluoride breakthrough curves for BC and AA PD-RSSCTs simulating full-scale (a) EBCTs of 10 and 20 minutes on a throughput basis and (b) operation time with two 10 minute EBCT beds in series.

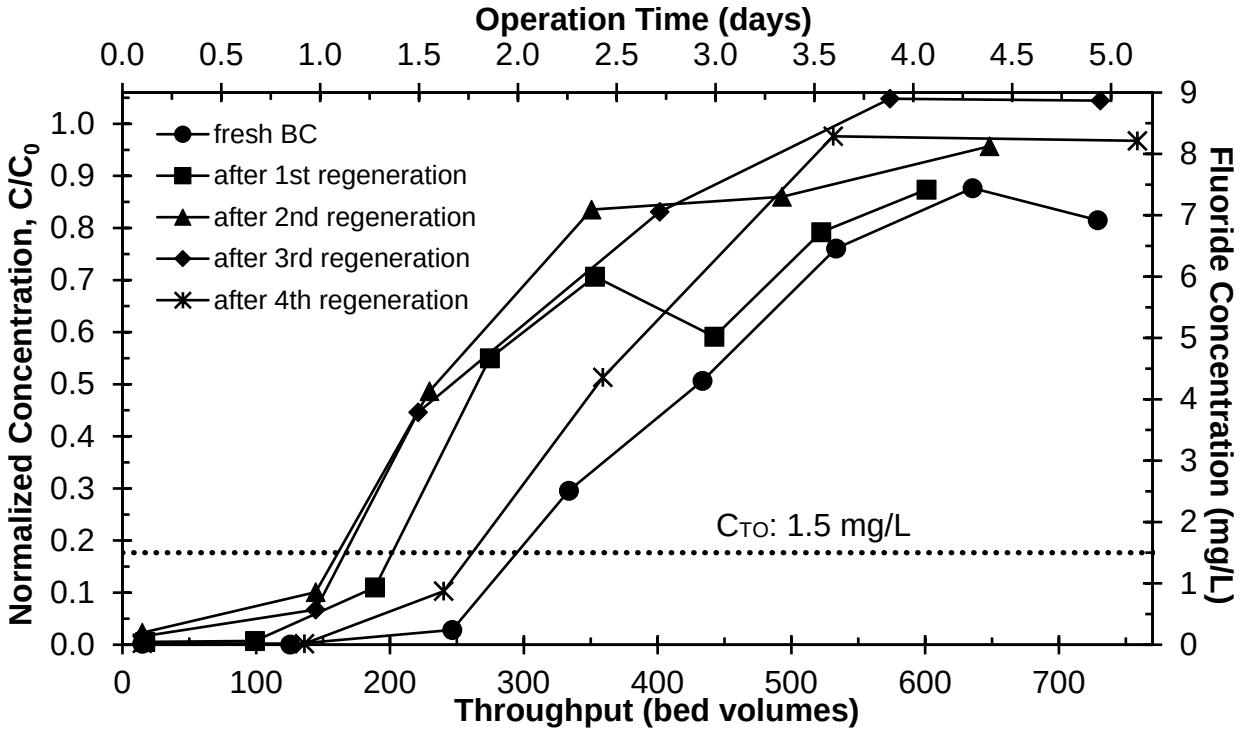

(a)

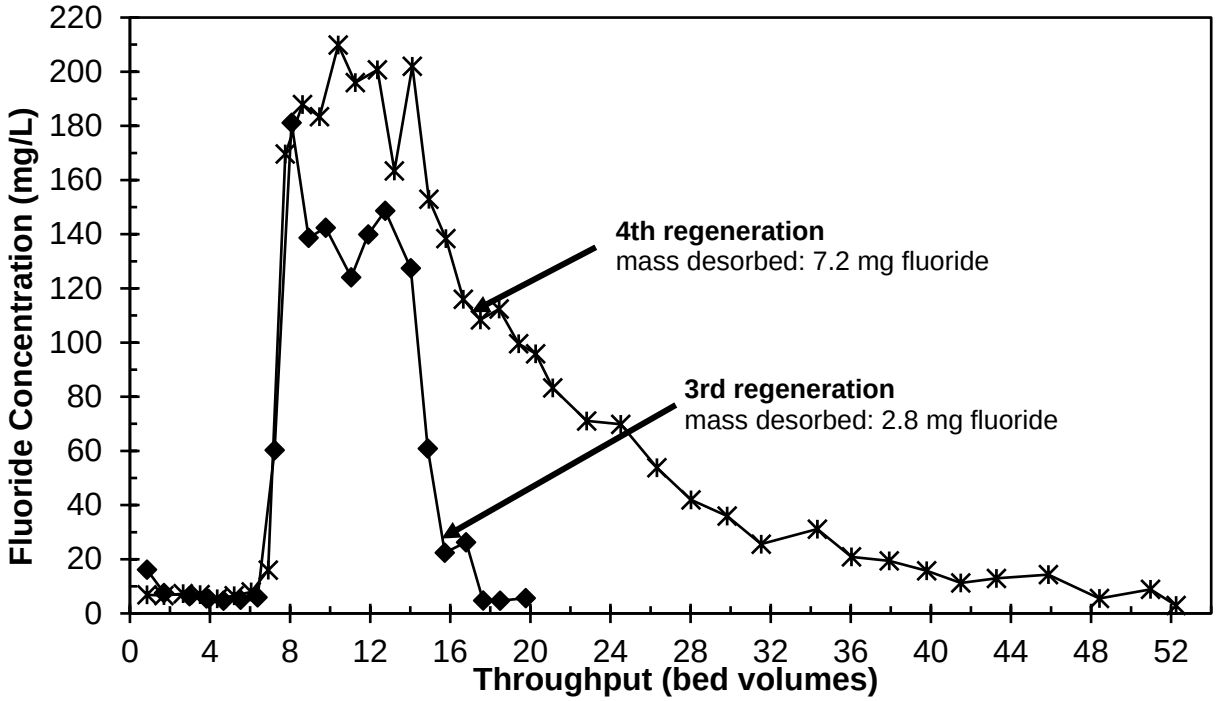

(b)

Figure 6. Fluoride BC PD-RSSCT (a) breakthrough curves before (fresh BC) and after several sodium hydroxide regenerations and (b) elution curves for the 3rd and 4th regenerations.

Tables

Table 1. Raw groundwater quality.

Parameter	Value	Units
Alkalinity	250±5	mg/L as $CaCO_3$
DOC	0.3±0.02	mg/L
Fluoride	8.5±0.2	mg/L
Hardness	11±0.1	mg/L as $CaCO_3$
pH	8.7±0.1	su
Sulfate	39±4	mg/L
TDS	565±58	mg/L
UVA_{254}	0.011±0.001	cm^{-1}

Note: DOC=dissolved organic carbon; TDS=total dissolved solids; UVA_{254}=ultraviolet absorbance at 254 nm. All parameters were measured at least twice.

840 *Table 2. Pilot column and RSSCT design and operational parameters for a full-scale EBCT of 10 minutes.*

Parameter	Units	BC			AA		
		Pilot Column	CD-RSSCT	PD-RSSCT	Pilot Column	CD-RSSCT	PD-RSSCT
d_{bed}	mm	25	9.5	4.8	25	9.5	4.8
d_p	mm	0.92	0.21	0.11	0.86	0.21	0.11
EBCT	min	10	0.5	1.2	10	0.6	1.3
HLR	m/h	1.0	4.3	6.7	1.0	4.0	6.7
L_{bed}	cm	17	3.8	13	17	4.1	14
Re·Sc	unitless	430	430	340	410	410	340
ϱ_{bed}	g/L	630	690	700	560	590	550
Runtime	hours	390	19	23	340	22	38
Flowrate	mL/min	8.4	5.1	2.0	8.4	4.8	2.0
Water	L	160	5.4	2.9	160	5.9	3.9

841 Note: d_{bed}=bed diameter; d_p=particle diameter; EBCT=empty bed contact time; HLR=hydraulic loading rate;
842 L_{bed}=bed length; Re·Sc=product of Reynolds and Schmidt numbers; ϱ_{bed}=bed density.
843

844 *Table 3. BC and AA surface area and pore volume analysis.*

Adsorbent	d_p (mm)	Surface Area (m^2/g)		Total Pore Volume (cm^3/g)		Average Pore Diameter (nm)	
		N_2	CO_2	N_2	CO_2	N_2	CO_2
BC	0.92	82	150	0.25	0.073	12	19
BC	0.21	87	-	0.25	-	12	-
BC	0.11	87	-	0.24	-	11	-
AA	0.86	350	450	0.44	0.21	5.3	19
AA	0.21	330	-	0.44	-	5.7	-
AA	0.11	330	-	0.45	-	5.8	-

845 Note: BC=bone char; AA=activated alumina. N_2 used BET equation. CO_2 used Dubinin-
846 Astakhov equation. For N_2, total pore volume is BJH adsorption cumulative volume of pores
847 between 1.7 and 300 nm. For CO_2, value represents limiting micropore volume.
848

Appendix B

Journal of Water Process Engineering – Accepted, Pre-Proof Manuscript

Application of Powdered Steel Slag for More Sustainable Removal of Metals from Impaired Waters

Anthony M. Kennedy and Miguel Arias-Paic

Abstract

Using abundant and cheap steel slag for metals removal from water represents an opportunity to recover waste material from one industry as a resource for another. In this study, powdered steel slag which contains lime (CaO) leftover from the steelmaking process, was evaluated and benchmarked against the relatively expensive and energy-intensive chemical sodium hydroxide (NaOH) for the removal of cadmium (Cd), manganese (Mn), and zinc (Zn) from two different mine drainage waters. Unlike isotherm and kinetic studies that represent most previous work, this study evaluated metals removal under realistic simulated water treatment conditions (doses, mixing, contact times, etc.), bringing the material one-step closer to actual full-scale implementation. In the neutral pH water with lower metals concentrations, approximately four times more steel slag (400 mg/L) compared to NaOH (100 mg/L) was required to achieve >70% metals removal. In the acidic pH water with higher metals concentrations, steel slag was insufficient to raise the pH at reasonable doses (<1,000 mg/L) but was shown to reduce NaOH dosing requirements by 25% (600 to 450 mg/L) when used in combination with steel slag (600 mg/L). Like NaOH, steel slag addition facilitated metal precipitate formation but also provided relatively high specific surface area (7.6 m^2/g) for metal adsorption, particularly for Mn, a promising finding for future work to evaluate sludge recycle. Water treated with steel slag was also found to be more amenable to 0.45 μm filtration than water treated with NaOH.

Introduction

Reclaiming waste materials from one industry as useful materials in another is is becoming increasingly attractive in a resource-limited world. One example, and the topic of this study, is the use of steel slag for the removal of metals from water. Steel slag is a waste byproduct from steelmaking, produced from the addition of burnt lime, or calcium oxide (CaO), to remove impurities (metal oxides, phosphorus) from the high temperature steelmaking process. As such, steel slag is a relatively high surface area and dense granular material rich in CaO and other metal oxides such as iron (III) oxide (Fe_2O_3) and silicon dioxide (SiO_2). In addition to having a high specific surface area, the presence of CaO in steel slag increases water pH (Feng et al. 2004, Caicedo-Ramirez et al. 2018) and divalent calcium (Ca^{2+}) concentrations through the formation of hydrated lime or calcium hydroxide ($Ca(OH)_2(s)$) as shown in Equation 1, a desirable trait for metals removal (e.g., as hydroxide precipitates) from water.

$$CaO(s) + H_2O \rightarrow Ca(OH)_2(s) \rightarrow Ca^{2+} + 2OH^- \quad (1)$$

Several studies have investigated the use of steel slag for metals removal from water, using either batch or fixed-bed scenarios. Fixed-bed steel slag studies are not discussed herein but have been shown to be effective at removing metals from water, albeit at relatively low water throughput (i.e., hundreds of bed volumes) (Gupta et al. 1997, Srivastava et al. 1997, Dimitrova 2002, Claveau-Mallet et al. 2013, Nguyen et al. 2018). In the case of batch studies, which are more relevant to this

study, steel slag particles ranging from 24 to 2,000 μm in diameter have been evaluated for metals removal via adsorption to its relatively high metal oxide surface area (0.4 to 107 m^2/g) (Dimitrova 1996, Gupta et al. 1997, Srivastava et al. 1997, Dimitrova and Mehanjiev 2000, Feng et al. 2004, Kim et al. 2008, Xue et al 2009, Nguyen et al. 2018).

In environmental systems, metals removal mechanisms can be difficult to isolate or identify. Nevertheless, in general, free divalent metal cation (Me^{2+}) adsorption to the heterogeneous steel slag surface is akin to adsorption to homogenous metal oxide surfaces following the generic adsorption shown in Equation 2 (Benjamin and Leckie 1981, Dzombak and Morel 1987, Stumm and Morgan 1996, Buamah et al. 2008, Kim et al. 2008),

$$\equiv SOH^0 + Me^{2+} = \equiv SOMe^+ + H^+ \text{ or } \equiv SOH^0 + Me^{2+} + H_2O = \equiv SOMeOH + 2H^+ \quad (2)$$

where $\equiv SOH^0$ is a neutral surface site, $\equiv SOMe^+$ and $\equiv SOMeOH$ are surface sites occupied by a divalent metal cation, and H^+ is the hydrogen ion (proton) released into solution. Considering steel slag addition would raise the pH as given by Equation 1, the formation of divalent metal oxides (MeO), hydroxides ($Me(OH)_2$), and/or carbonates ($MeCO_3$) followed by precipitation to the steel slag surface could be expected in addition to metal-ligand complex (MeL) adsorption, or ternary surface complex formation, as shown in Equation 3 (Dzombak and Morel 1987, Stumm and Morgan 1996),

$$\equiv SOH^0 + Me^{2+} + L^- = \equiv SOMeL^0 + H^+ \quad (3)$$

where L^- is a ligand (e.g., OH^-) that acts as a bridge to form $\equiv SOMeL^0$, a neutral surface site occupied by the metal-ligand complex.

In prior batch equilibrium adsorption studies, steel slag was shown to be an effective adsorbent for removing several divalent cationic metals from solution, namely cadmium (Cd), copper (Cu), lead (Pb), nickel (Ni), zinc (Zn) (Dimitrova 1996, Gupta et al. 1997, Srivastava et al. 1997, Dimitrova and Mehanjiev 2000, Feng et al 2004, Kim et al. 2008, Xue et al. 2009, Nguyen et al. 2018). Increased adsorption was measured at higher pH values above the steel slag surface pH point of zero charge (pH_{pzc}), where the negative surface charge attracted divalent cations. However, these studies controlled pH using either acid or base addition as opposed to testing pH response derived solely from steel slag addition. Most solutions were synthetic (buffered deionized water) with high steel slag doses and metals concentrations, 10,000 mg/L and 500 mg/L, respectively, as an example (Gupta et al. 1997). Work by Nguyen et al. (2018) evaluated adsorption of metals to steel slag under more realistic scenarios (doses and metals concentrations of 100 mg/L and 5 mg/L, respectively), but experiments were still run to equilibrium (24 hours) at a constant pH (6.5). More research with real waters, reasonable steel slag doses, and typical contact times (minutes to hours) is needed to evaluate the potential of steel slag as a practical, and potentially more sustainable, water treatment process. As with any novel material, a baseline comparison to existing treatment chemicals is needed, but such comparisons are also lacking in previous studies. Therefore, the objective and novelty of this study was to evaluate steel slag performance, benchmarked against relatively expensive and energy-intensive NaOH, under realistic treatment plant conditions with two real waters, both relatively high in Cd, manganese (Mn), and Zn. Experiments were designed to determine bulk performance of steel slag, as measured by metals removal, when added during water treatment processes similar to adsorbents such as powdered activated carbon (PAC), as opposed to experiments designed to elucidate specific removal mechanisms, surface reactions, or kinetic parameters.

Materials and Methods

936 **Waters**
937 Two mine drainage waters with elevated levels of metals were tested in this study, one from the
938 Leadville Mine Drainage Tunnel (LMDT) in Leadville, Colorado, and one from the Argo Tunnel
939 (AT) in Idaho Springs, Colorado. Both LMDT and AT have operating water treatment plants that
940 use NaOH and $Ca(OH)_2$ to remove metals prior to discharging to the vulnerable surface waters of
941 the Arkansas River and Clear Creek, respectively. Most testing was performed with LMDT water,
942 but for both waters testing was either performed at the respective water treatment plants or after
943 collecting water in 20 L HDPE containers and storing at 4°C until use within a week. Relevant raw
944 water quality of the two waters is shown in Table 1, highlighting the metals focused on in this study:
945 Cd, Mn, and Zn, due to difficulties in removal solely through increases in pH compared to other
946 source water metals (Cu, Fe, Pb). Historically, LMDT water is atypical for mine drainage, in that it is
947 influenced by native groundwater, which raises pH, alkalinity, and oxidation reduction potential
948 (ORP). LMDT water has significant alkalinity, neutral pH, and relatively low metals concentrations.
949 By contrast, AT water is historically more typical of acid mine drainage, exhibiting low pH, no
950 alkalinity, and relatively high concentrations of metals.
951
952 **Slag**
953 Basic oxygen furnace steel slag, the same product used by Caicedo-Ramirez et al. (2018, 2019) was
954 tested in this study. Major metal oxide composition of this steel slag, identified using powder X-ray
955 diffraction (XRD), was performed by Caicedo-Ramirez et al. (2019) and consisted of CaO (32%),
956 Fe_2O_3 (26%), SiO_2 (15%), magnesium oxide (MgO, 11%), aluminum oxide (Al_2O_3, 6.6%),
957 manganese oxide (MnO, 2.5%), phosphorus pentoxide (P_2O_5, 0.7%), calcium or sodium sulfate
958 ($CaSO_4$ or Na_2SO_4, 0.4%) and sodium oxide (Na_2O, 0.1%), consistent with steel slag composition
959 (Dimitrova and Mehanjiev 2000, Feng et al. 2004, Xue et al. 2008, Nguyen et al. 2018). To create a
960 powder similar in size to PAC, small batches (~100 g) of as-received steel slag (<1.6 mm) were
961 sieved to particle diameters less than 75 μm using a stainless steel sieve (US Standard Mesh #200)
962 and vibratory sieve shaker. Powdered steel slag stock slurries (20 g/L) were made several times over
963 the course of testing using deionized water (resistivity >16 MΩ·cm). Stock slurries were stored at
964 room temperature in 1 L amber glass bottles.
965 Scanning electron microscopy (SEM) paired with energy-dispersive X-ray spectroscopy
966 (EDS) of steel slag surfaces was also performed to obtain relative mass percent values of identified
967 elements with a detection limit of 0.1% (Rocky Mountain Laboratories, Inc., Colorado). An SEM
968 image of the powdered raw steel slag is shown in Figure 1 and demonstrates a rough surface
969 morphology that contributed to a measured specific surface area value of 7.6 m^2/g, according to the
970 Brunauer-Emmett-Teller (BET) method (Micromeritics Instrument Corporation, Georgia). For
971 reference, the specific surface area of a perfectly spherical steel slag particle with a diameter of 38
972 μm (half of 75 μm) and solid particle density (ρ_s) of 2.6±0.3 g/cm (Dimitrova 1996, Gupta et al.
973 1997, Srivastava et al. 1997) would be approximately 0.06 m^2/g, or nearly 130 times less surface area
974 than what was measured for the steel slag used in this study.
975 To eliminate the ability of as-received steel slag to increase water pH and subsequently test
976 that modification, approximately 5 g of powdered steel slag was exhausted for pH change capacity
977 by up-flowing deionized water (pH~6, 10 mL/min) through a small fluidized bed of steel slag in 9.5
978 mm (inside diameter) polypropylene tubing using a diaphragm pump. When the fluidized bed
979 effluent water reached a steady-state pH value of approximately 7 after several months of operation,
980 the process was stopped. Powdered steel slag was removed from the tubing, dried in a muffle
981 furnace at 100°C, and stored in a 50 mL glass beaker until use. Herein, this steel slag is referred to as

exhausted slag (ES) and steel slag added from the previously described stock slurry is referred to as unexhausted slag (UES).

Sodium Hydroxide

As a benchmark for performance, all UES and ES tests included parallel tests with NaOH. NaOH was chosen instead of pure CaO or $Ca(OH)_2$ because it contributes only hydroxide ions (OH^-) to solution (i.e., pH increase only), whereas CaO or $Ca(OH)_2$ contribute Ca^{2+} and OH^- (Equation 1) such that metals removal could be enhanced through coprecipitation with and/or adsorption to calcium carbonate ($CaCO_3(s)$) (Stumm and Morgan 1996). Both LMDT and AT waters did contain appreciable amounts of Fe (>1.5 and >15 mg/L, respectively), in which case some metals removal would also be expected through adsorption to iron (III) hydroxide ($Fe(OH)_3(s)$) surfaces, formed from the addition of NaOH (Stumm and Morgan 1996). NaOH stock solutions were made several times over the course of testing using reagent grade pellets (Fisher Scientific, New Hampshire) and deionized water. Stock solutions were stored at room temperature in 1 L amber glass bottles.

Jar Testing

All testing was performed using a jar tester (Phipps & Bird, Inc., Virginia) with 2 L clear acrylic square jars. For jar testing, UES (added from stock slurry), ES (added dry), or NaOH (added from stock solution) were added using small measuring cups or plastic syringes during a 1 to 2 minute rapid mix phase with an average velocity gradient (G) value of approximately 350 s^{-1} followed by a 60 minute slow mix phase with a G value range of 50 to 90 s^{-1}. Upon completion of the slow mix phase, samples were immediately removed from the built-in jar valve and filtered using 0.45 μm acrylic copolymer membrane disc filters (Pall Corporation, New York). Metals removal kinetics were evaluated in a separate set of jar tests under the same conditions and procedures, where metals samples were collected and filtered after 10, 30, 60, and 120 minutes of slow mixing. These times were chosen based on the relevance to typical time scales of water treatment plants. Following another set of jar tests, filterability of water treated with either UES or NaOH was evaluated. Filterability was defined as the time to filter 500 mL of water through the same 0.45 μm filter under a constant 80 kPa of vacuum pressure immediately following the slow mix phase, similar to the silt density index (SDI) test (ASTM D4189).

Water Quality Analysis

Dissolved Cd, Mn, and Zn were measured according to EPA Method 200.8 by a certified laboratory (Green Analytical Laboratories, Colorado) with minimum reporting levels (MRL) of 0.0001, 0.0005, and 0.002 mg/L, respectively, for LMDT water and 0.002, 0.01, and 0.04 mg/L, respectively, for AT water. Other metals of interest were measured according to either EPA Method 200.7 or 200.8 by the same certified laboratory. Alkalinity was measured using Hach Method 8203 (Hach, Colorado). pH was measured using a gel-filled electrode attached to a portable multimeter (Hach, Colorado), calibrated before each jar test. Turbidity was measured using a turbidimeter (Hach, Colorado). Hardness and ORP in Table 1 were obtained from historical LMDT data.

Results and Discussion

Dose Response

Final pH measured after 60 minutes of slow mixing, as a function of UES and NaOH dose, is shown in Figure 2a for LMDT water. Although not shown, within the first few minutes of slow mixing significant floc formation was visible in both UES and NaOH jars. As expected, NaOH was very effective at raising the pH compared to UES, confirming its use as a performance benchmark.

As a point of reference, every 1.0 mg/L of NaOH theoretically adds 0.43 mg/L as OH^- to solution while every 1.0 mg/L of CaO theoretically adds 0.61 mg/L as OH^- (Equation 1). However, considering UES was approximately 32% CaO, only 0.20 mg/L as OH^- would have been added to solution assuming complete dissolution. Therefore, to reach the same pH, it would be expected the UES dose would need to be at least twice the NaOH dose. As shown in Figure 2a, approximately four to ten times UES was required to reach a similar final pH, driven by a relative plateau starting at a UES dose of 200 mg/L. Plateauing pH indicates buffering, an example being silicic acid (H_4SiO_4, pK_{a1} 9.8, pK_{a2} 13.2) formation from the dissolution of $SiO_2(s)$ (Dimitrova and Mehanjiev 2000, Caicedo-Ramirez et al. 2018), but as a check, alkalinity was measured at UES doses of 400 and 1,000 mg/L. Raw water alkalinity decreased from 120±5 mg/L as $CaCO_3$ to final values (after 60 minutes of slow mixing) of 105±5 and 70±5 mg/L as $CaCO_3$, respectively. From this data alone it is unclear why final pH plateau behavior was observed for UES, but a decrease in alkalinity is consistent with precipitation of $Me(OH)_n(s)$ and $MeCO_3(s)$ complexes. One hypothesis as to why the final pH plateaued is release of H^+ with free metal cation or metal-ligand complex adsorption (Equations 2 and 3) increasingly counteracted the effect of OH^- addition (Equation 1). Another related effect may be that increasing UES dose increased precipitation and/or adsorption of $Me(OH)_n(s)$ and $MeCO_3(s)$ complexes, such as $CaCO_3(s)$, that coated the UES surface inhibiting further dissolution of CaO that would have increased the pH (Equation 1).

Ultimately, the dissolution of CaO from UES and subsequent increase in pH led to increased metal adsorption and precipitate formation such that particles were filterable using a 0.45 μm filter. Normalized dissolved metals concentrations, or the final concentration (C) divided by the initial raw water concentration (C_0), as a function of increasing UES and NaOH doses are shown in Figure 2b for LMDT water. For both UES and NaOH, metals removed increased with dose and the percent removal followed Zn>Cd>Mn, consistent throughout all testing and at least with the solubility order of Cd and Zn $MeCO_3(s)$, $Me(OH)_2(s)$, and MeO(s) complexes (Stumm and Morgan 1996). While the removal of Cd and Zn through precipitate formation from increasing pH is common using either CaO or NaOH, Mn removal through precipitate formation is commonly and alternatively achieved through oxidation as manganese dioxide ($MnO_2(s)$), likely because the reaction kinetics are faster than precipitation as $Mn(OH)_2(s)$ or $MnCO_3(s)$ (Figure SM2). It is difficult to compare these results to published literature as these experiments were somewhat unique due to prior adsorption studies having very high steel slag doses, >1,000 mg/L, and run until equilibrium (Dimitrova 1996, Gupta et al. 1997, Srivastava et al. 1997, Dimitrova and Mehanjiev 2000, Feng et al. 2004, Kim et al. 2008, Xue et al 2009).

Using modeling software (Stream Analyzer, OLI Systems, Inc., New Jersey) to generate E_h-pH diagrams with the LMDT raw water quality in Table 1 as inputs (Figure SM1 through Figure SM3 in Supplementary Material), the following metal precipitates were predicted to form under equilibrium and testing conditions (positive ORP, high pH, 2+ oxidation state for Cd, Mn, and Zn): cadmium carbonate ($CdCO_3(s)$), cadmium hydroxide ($Cd(OH)_2(s)$), manganese carbonate ($MnCO_3(s)$), manganese hydroxide ($Mn(OH)_2(s)$), zinc carbonate ($ZnCO_3(s)$), and zinc oxide (ZnO(s)). Considering UES would contribute more species to solution than NaOH based on its metal oxide composition, the formation of additional precipitates such as $Al(OH)_3(s)$, $MgCO_3(s)$, or $SiO_2(s)$ was also possible. The potential for precipitation of several $Me(OH)_n(s)$ and $MeCO_3(s)$ complexes would be consistent with the observed decrease in alkalinity with increase in UES dose. For further testing, results shown in Figure 2b were used to establish a UES dose of 400 mg/L and NaOH dose of 100 mg/L as they provided similar and high levels (>70%) of Cd, Mn, and Zn removal. It should be noted that duplicate jars in one test measured release of dissolved Ca (65 to 85±3.3 mg/L) and Si (5.4 to 6.3±0.25 mg/L) at the UES dose of 400 mg/L, confirming dissolution from UES and availability to form precipitates in solution (e.g., $CaCO_3(s)$) and potentially buffer pH.

The combination of data in Figures 2a and 2b is shown in Figure 2c, with normalized dissolved metals concentrations shown as a function of final pH. As expected, metals removal increased with increasing pH, with more similar trends between UES and NaOH than those shown in Figure 2b. It is difficult to compare these results to published literature adsorption studies that relied on added acid/bases to reach target pH values instead of steel slag induced pH change. In general, Cd and Zn were more easily removed at lower pH values than Mn, as was observed in Figure 2b as a function of dose. Interestingly, each metal exhibited a crossover point after which UES addition resulted in higher metals removal compared to NaOH at the same final pH value. These pH crossover points are specifically called out in Figure 2c and were approximately 7.8, 9.0, and 8.0 for Cd, Mn, and Zn, respectively. The change was most dramatic for Mn, where approximately 70 to 75% removal was reached at pH 9.1 with UES but required pH 9.7 with NaOH. Because metals removal was higher with UES at a lower pH than NaOH following the crossover point, such behavior suggests adsorption to the UES surface as a removal mechanism, in addition to metal precipitate formation followed by size exclusion during filtration.

Kinetics

Based on the dose response curves in Figure 2b, UES and NaOH doses of 400 and 100 mg/L, respectively, were used for additional testing to establish metals removal kinetics. Normalized dissolved metals concentrations as a function of slow mixing time are shown in Figure 3 for LMDT water. Removal curves in Figure 3 confirm the selected doses for UES and NaOH provided similar removal of Cd, Mn, and Zn in the expected removal percentages (Zn>Cd>Mn). The curve shapes are similar, suggesting similar removal mechanisms of adsorption and precipitation of metals to UES and metal oxide floc surfaces. Initial kinetics were relatively fast, with most of the Cd, Mn, and Zn removed within the first 10 minutes. In the case of UES (similar for NaOH), 86, 43, and 98% removal of Cd, Mn, and Zn, respectively, occurred within the first 10 minutes. For the next 110 minutes, an additional 10, 30, and 1% removal of Cd, Mn, and Zn, respectively, was realized using UES, again indicating slower kinetics for Mn precipitate formation. Removal coincided with final pH, where the pH did not significantly increase further after the 10-minute sample (9.3±0.1 for UES and 9.9±0.2 for NaOH). Similar results to those shown in Figure 3, albeit at much higher Cd and Zn concentrations (>23 and >35 mg/L, respectively) and steel slag doses (>1,000 mg/L) have been observed, with an initial rapid removal stage followed by a gradual removal stage (Dimitrova 1996, Gupta et al. 1997, Xue et al. 2009). A two-step adsorption process is typical for adsorption of metals to metal oxide surfaces (Benjamin and Leckie 1981, Dzombak and Morel 1987, Davies and Morgan 1989) and therefore, more gradual removal following the initial rapid phase may have been more related to metal-ligand complex adsorption to the UES and metal oxide surfaces (Equation 3). Adsorption is precluded, and typically rate limited by, film diffusion to the surfaces as opposed to solely precipitate growth into a filterable particle or floc, a process that can be very fast as water molecules leave the metal coordination sphere (Benjamin and Leckie 1981, Stumm and Morgan 1996).This postulation is unresolved as tests in this study were not designed to elucidate kinetics specific to different removal mechanisms.

Adsorption

Thus far, it has been shown that greater metals removal from LMDT water was measured with increasing UES and NaOH doses (i.e., with increasing pH), with specific removal mechanisms difficult to discern. To better isolate adsorption of free metal cations (Equation 2) and metal-ligand complexes (Equation 3) as a potential removal mechanism, different ES doses were tested in conjunction with a constant NaOH dose of 30 mg/L, which resulted in a consistent final pH of 9.4±0.1 for all experiments. ES was mostly exhausted for its pH change capacity, so its addition

intentionally did not increase pH to any measurable degree but did add significant surface area for metal adsorption and/or precipitation. Results of ES testing are shown in Figure 4, where normalized dissolved metals concentrations are presented as a function of ES dose and surface area added. At a NaOH dose of 30 mg/L only, with no ES added, Cd, Mn, and Zn removal were 75, 19, and 98%, respectively. For Cd and Mn, removal increased significantly with increasing ES dose, while Zn removal was relatively stable at 97 to 98% as it was the most easily removed constituent with elevated pH (Figure 2c and Figure 3). At a ES dose of 200 mg/L, Cd and Mn removal improved to 84 and 46%, respectively, presumably through adsorption to the added ES surface area of approximately 1.5 m^2/L or 3.0 m^2 for a 2 L jar. Mn dose response was the most dramatic and somewhat expected based on known affinities of Mn for iron (III) oxide surfaces (e.g., α-FeOOH) (Davies and Morgan 1989, Buamah et al. 2008). These results are also consistent with the stark crossover point in Figure 2c for Mn, where adsorption to the UES surface was postulated since removal was greater than NaOH tests at the same pH values greater than 9.0.

In addition to the jar test results shown in Figure 4, EDS analysis of surfaces for six different steel slag particles before (unused) and after (used) testing with LMDT water is shown in Table 2 (EDS spectra in Figure SM4 through Figure SM21 in Supplementary Material). For each element across the six different particles in Table 2, Tukey's Test was applied to establish differences in relative elemental surface mass percent values, termed values for short in this section, at the 95% confidence level. The six particles were (1) UES unused, (2) UES used at 400 mg/L, (3) ES unused dominated by Ca, (4) ES used at 200 mg/L dominated by Ca, (5) ES unused dominated by Fe, and (6) ES used at 200 mg/L dominated by Fe. The two ES particles were differentiated in Table 2 because it was apparent from SEM backscatter images (heavier elements are lighter in contrast) that ES particles were heterogeneous, one was dominated by Ca (darker in contrast) and another by Fe (lighter in contrast). On all six particle types, a Cd peak in the EDS spectra was not discernable from method noise, likely because of its low concentration compared to other metals.

For UES particles, differences in values between unused and used were significant only for carbon (C) and sulfur (S). S content was minimal in both cases, but the increase in C could have been from adsorption and/or precipitation of $MeCO_3$(s) complexes (e.g., $CaCO_3$(s)) to the UES surface. Although insignificant at the 95% confidence level, Mn values did increase on the UES surface from 0.4% (unused) to 0.6% (used), consistent with previous discussions on Mn adsorption, particularly the crossover points in Figure 2c. A discernable Zn peak in the EDS spectrum was not apparent for unused UES, but was for used UES at 0.6%, providing evidence for Zn adsorption and/or precipitation to the UES surface, consistent with the affinity of Zn for iron (III) oxide surfaces (e.g., $Fe_2O_3 \cdot H_2O$(am)) (Benjamin and Leckie 1981).

For Ca-dominated ES particles, there was not much difference in values between unused and used other than Zn, which increased from no discernable peak to 2.5%. Similar results were observed for Zn on unused and used Fe-dominated ES particles. Although insignificant at the 95% confidence level, Mn values for Ca-dominated ES particles were higher than UES values at 1.3%. Perhaps the most important values in Table 2 were for Mn on Fe-dominated ES particles. Mn values were 1.9 and 3.5% on the unused and used Fe-dominated particles, respectively, again consistent with previous studies that demonstrated Mn affinity for iron (III) oxide surfaces (Davies and Morgan 1989, Buamah et al. 2008). A value of 3.5% was significantly different at the 95% confidence level compared to UES and Ca-dominated ES values for Mn. These results further corroborate Mn adsorption to ES particles shown graphically in Figure 4.

Filterability and leaching

Throughout all testing, floc settling rates were visually faster in UES- than NaOH-treated jars, where the addition of UES appeared to provide benefits similar to ballasted flocculation using microsand.

To formally evaluate settling rates, UES and NaOH settling tests were performed by measuring the turbidity of water pulled from the built-in jar values after 0, 5, 10, 15, 30, and 60 minutes of settling. However, turbidity results did not agree with visual observations or filter time for metals samples. UES treated water was visibly much clearer after as little as 5 minutes of settling but resulted in similar settled water turbidity values as NaOH treated water (e.g., 4.4±1.4 and 6.0±2.6 NTU, respectively, after 60 minutes). It is well-known jar tests are not ideal for evaluating floc settling due to the lack of depth and continued water movement once mixing stops compared to full-scale sedimentation basins. Therefore, as an alternative way to quantitatively establish the water clarity, or treatability, of UES- and NaOH-treated waters, filterability tests at the same doses of 400 and 100 mg/L, respectively, were performed. Filterability tests confirmed that water treated with UES was easier to filter immediately following 60 minutes of slow mixing, consistent with visual observations from settling tests. Specifically, triplicate tests established 4.3±0.1 minutes to filter 500 mL using UES (final pH 9.5±0.0) and nearly three times longer, or 11.9±2.7 minutes, using NaOH (final pH 10.2±0.1).

These results clearly indicate floc particles formed from NaOH addition had a higher affinity for the hydrophilic filter surface compared to floc/UES particles formed from UES addition. That increased affinity materialized as a fouling layer, increasing resistance to water flow despite a constant applied vacuum pressure. Without zeta potential or streaming current measurements it is difficult to assume floc particle surface charges following NaOH or UES addition, but filterability tests operationally demonstrated there were considerable differences in floc character and behavior. Considering the abundance of species that can dissolve from the UES surface (e.g., Ca and Si) and form precipitates (e.g., $CaCO_3(s)$ and $SiO_2(s)$), these results are not entirely surprising. Independent of floc affinity for the filter surface, the vast majority of UES particles (<75 μm) would be filterable using a 0.45 μm filter. As a result, LMDT water treated with UES may also have been easier to filter due to adsorption of free metal cation and metal-ligand complexes to UES surface, as opposed to their precipitation in solution that could contribute to a fouling layer at the filter surface. Future research could elucidate the difference in filtration between the two treated waters and extend results to design of a downstream process such as membrane filtration.

Following filterability tests, duplicate jar samples were analyzed for dissolved arsenic (As), chromium (Cr), cyanide (CN^-), phosphorus (P), selenium (Se), and sulfur (S) over concerns related to the leachability of undesirable constituents from UES. As, CN^-, P, and Se were all below MRLs of 0.001, 0.010, 0.050, and 0.001 mg/L, respectively, in raw and UES treated water. Cr concentrations decreased slightly from 0.0017 mg/L in the raw water to 0.0011±0.0001 mg/L in the UES treated water. S also decreased slightly from 71 mg/L in the raw water to 69±0.2 mg/L in the UES treated water. Therefore, for this UES and LMDT water combination, leaching of concerning constituents was not significant. However, although the same constituents were not measured in AT treated water, leaching could be more significant in acid mine drainage waters.

Combined Treatment

While UES addition alone was sufficient to significantly raise the pH of LMDT water, it was unable to do the same in the much more acidic AT water. For example, at a dose of 2,400 mg/L, UES raised AT water pH from 2.9 to 6.0, resulting in only 21, 15, and 30% removal of Cd, Mn, and Zn, respectively. Therefore, UES was tested in conjunction with NaOH as a means to reduce NaOH dosing requirements, a relatively expensive chemical compared to steel slag. Recent costs for NaOH and steel slag were approximately $1.15 per kg NaOH (Kennedy, personal communication) and $0.03 per kg steel slag (USGS 2020). Results comparing NaOH alone with a NaOH dose of 450 mg/L combined with varying UES doses is shown in Figure 5 for Mn. Only Mn data are shown because as previously demonstrated, it was the most difficult to remove and present at a

concentration much higher than LMDT water at approximately 65 mg/L. A NaOH dose of 450 mg/L was chosen to target approximately 50% Mn removal, based on preliminary testing, but removed Cd and Zn to >97%, which is the reason for their omission in Figure 5.

As shown in Figure 5, a NaOH dose of 450 mg/L (at 0 mg/L on UES/NaOH curve or interpolated point on NaOH only curve with dashed lines) was close to the target, resulting in Mn removal of approximately 44%. Mn removal increased with UES dose and intersected the NaOH only curve at approximately 600 mg/L. As such, this point can be interpreted as a NaOH dose reduction of 150 mg/L (25%) with the addition of 600 mg/L UES. Similar interpretations can be made using interpolations of both curves, demonstrating that UES use could result in significant reductions of NaOH dosing requirements. For example, if 80% Mn removal was required, it could be accomplished with approximately 550 mg/L NaOH or 450 mg/L NaOH with 350 mg/L UES, an 18% reduction in NaOH. Considering metals removal was observed using NaOH and ES (Figure 4), sludge recycle is likely to increase metals removal if such a process were implemented. An additional observation of note in Figure 5 is no Mn removal was observed by solely dosing NaOH at 300 mg/L (pH 6.8), but as previously stated, approximately 15% Mn removal was observed at the high UES dose of 2,400 mg/L (pH 6.0). Such behavior further supports the adsorption of Mn to the UES surface as a removal mechanism.

Conclusions

Two different types of the same original steel slag, UES and ES, were applied under simulated water treatment conditions for the removal of metals from two mine drainage waters, one neutral and one acidic. Approximately four times as much UES (400 mg/L) compared to NaOH (100 mg/L) was required to achieve >70% removal of Cd, Mn, and Zn from near neutral pH LMDT water. Beyond pH values specific to each metal, UES provided better removal at lower pH values compared to NaOH, which was attributed to metal adsorption to the UES surface. Most metals removal occurred within the first 10 minutes of UES (400 mg/L) and NaOH (100 mg/L) addition, however, continued removal was observed over the next 110 minutes, especially for Mn. At a constant pH value of 9.4 (30 mg/L NaOH), increased addition of ES (0 to 200 mg/L) increased metals removal, confirming adsorption was a significant removal mechanism in addition to removal via filtration of metal precipitates. These results also indicate that in a full-scale process, sludge recycle could be implemented to enhance metals adsorption and reduce UES dose requirements. EDS analysis also confirmed metal adsorption through relative quantification of UES and ES surface concentrations. LMDT water treated with UES was easier to filter than water treated with NaOH based on time to filter 500 mL through 0.45 μm filters, which deserves further research into specific floc-filter interactions. For the very acidic AT water, UES (600 mg/L) was able to reduce NaOH dose requirements by 25% (600 to 450 mg/L) to achieve ~90% Mn removal. Compared to NaOH, UES represents a significant opportunity to use a waste material to sustainably reduce metals removal treatment costs. For that reason, future research should test steel slag at the pilot-scale with sludge recycle to evaluate full-scale feasibility.

References

Benjamin, M.M., Leckie, J.O. 1981. Multiple-site adsorption of Cd, Cu, Zn, and Pb on amorphous iron oxyhydroxide. Journal of Colloid and Interface Science, 79(1), 209–221.

Buamah, R., Petrusevski, B., Schippers, J.C. 2008. Adsorptive removal of manganese(II) from the aqueous phase using iron oxide coated sand. Journal of Water Supply: Research and Technology–AQUA, 57(1), 1–11.

Caicedo-Ramirez, A., Hernandez, M.T., Grubb, D.G. 2018. Elution history of basic oxygen furnace slag to produce alkaline water for reagent purposes. Proceedings of the Protection and Restoration of the Environment XIV International Conference, 1095–1103.

Caicedo-Ramirez, A., Laroco, N., Bilgin, A.A., Shiokari, S., Grubb, D.G., Hernandez, M. 2019. Engineering addition of slag fines for the sequestration of phosphate and sulfide during mesophilic anaerobic digestion. Water Environment Research, 92(3), 455–464.

Claveau-Mallet, D., Wallace, S., Comeau, Y. 2013. Removal of phosphorus, fluoride and metals from a gypsum mining leachate using steel slag filters. Water Research, 47(4), 1512–1520.

Davies, S.H.R. Morgan, J.J. 1989. Manganese(II) oxidation kinetics on metal oxide surfaces. Journal of Colloid and Interface Science, 129(1), 63–77.

Dimitrova, S.V. 1996. Metal sorption on blast-furnace slag. Water Research, 30(1), 228–232.

Dimitrova, S.V. Mehanjiev, D.R. 2000. Interaction of blast-furnace slag with heavy metal ions in water solutions. Water Research, 34(6), 1957–1961.

Dimitrova, S.V. 2002. Use of granular slag columns for lead removal. Water Research, 36(16), 4001–4008.

Dzombak, D.A., Morel, M.M. 1987. Adsorption of inorganic pollutants in aquatic systems. Journal of Hydraulic Engineering, 113(4), 430–475.

Feng, D., van Deventer, J.S.J., Aldrich, C. Removal of pollutants from acid mine wastewater using metallurgical by-product slags. Separation and Purification Technology, 40(1), 61–67.

Gupta, V.K., Rastogi, A., Dwivedi, M.K., Mohan, D. 1997. Process development for the removal of zinc and cadmium from wastewater using slag–a blast furnace waste material. Separation Science and Technology, 32(17), 2883–3912.

Kennedy, A.M. Email communication with LMDT water treatment plant supervisor on March 4, 2020: $523 per wet ton of 50% sodium hydroxide, ~3,500 gallon delivery.

Kim, D.H., Shin, M.C., Choi, H.D., Seo, C.I., Baek, K. 2008. Removal mechanisms of copper using steel-making slag: adsorption and precipitation. Desalination, 223(1–3), 283–289.

Nguyen, T.C., Loganathan, P., Nguyen, T.V., Kandasamy, J., Naidu, R., Vigneswaran, S. 2018. Adsorptive removal of five heavy metals from water using blast furnace slag and fly ash. Environmental Science and Pollution Research, 25, 20430–20438.

Srivastava, S.K., Gupta, V.K., Mohan, D. 1997. Removal of lead and chromium by activated sludge–a blast-furnace waste. Journal of Environmental Engineering, 123(5), 461–468.

Stumm, W., Morgan, J.J. 1996. Aquatic Chemistry: Chemical Equilibria and Rates in Natural Waters, 3rd Edition. John Wiley & Sons, Inc., New York.

United States Geological Survey (USGS). 2020. Iron and Steel Slag Statistics and Information. National Minerals Information Center. https://www.usgs.gov/centers/nmic/iron-and-steel-slag-statistics-and-information?qt-science_support_page_related_con=0#qt-science_support_page_related_con. Accessed March 4, 2020.

Xue, Y., Hou, H., Zhu, S. 2009. Competitive adsorption of copper(II), cadmium(II), lead(II), and zinc(II) onto basic oxygen furnace slag. Journal of Hazardous Materials, 162(1), 391–401.

Figures

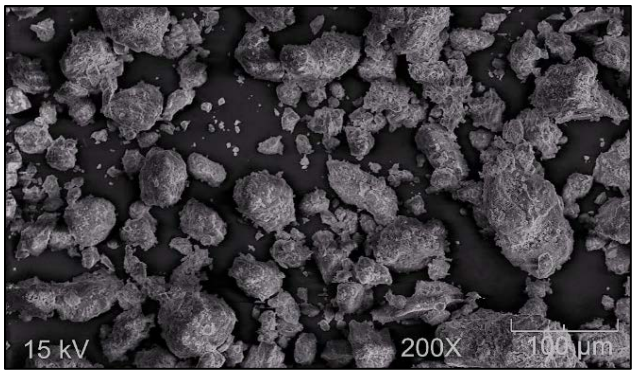

Figure 1. SEM image of unused UES.

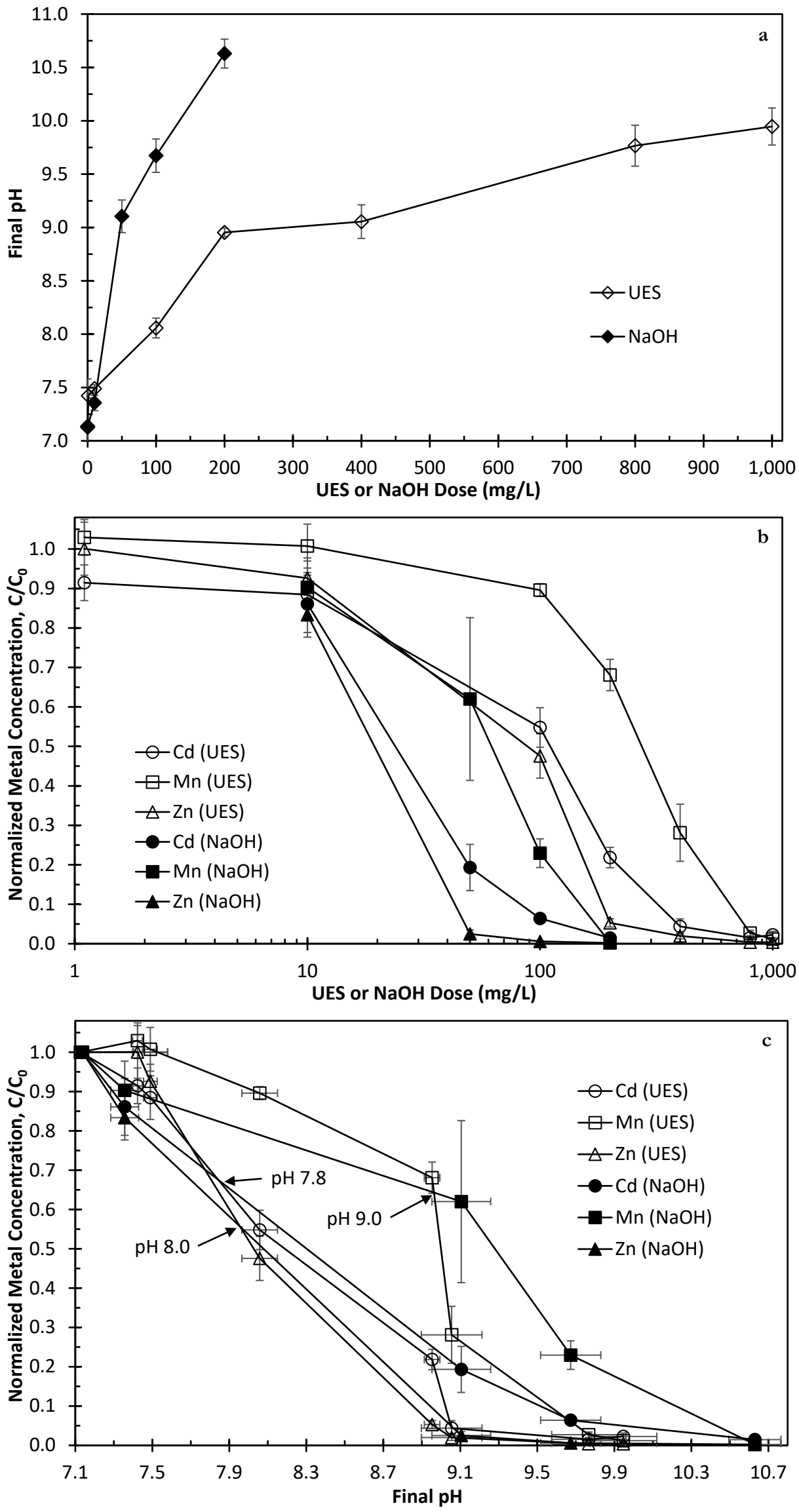

Figure 2. UES and NaOH dose response comparisons in LMDT water: (a) final pH as a function of dose, (b) normalized dissolved metals concentration as a function of dose, and (c) normalized dissolved metals concentration as a function of final pH. Error bars represent the standard deviation of at least triplicate jar tests. Cd0: 0.0062±0.0013 mg/L, Mn0: 1.2±0.16 mg/L, Zn0: 1.8±0.24 mg/L.

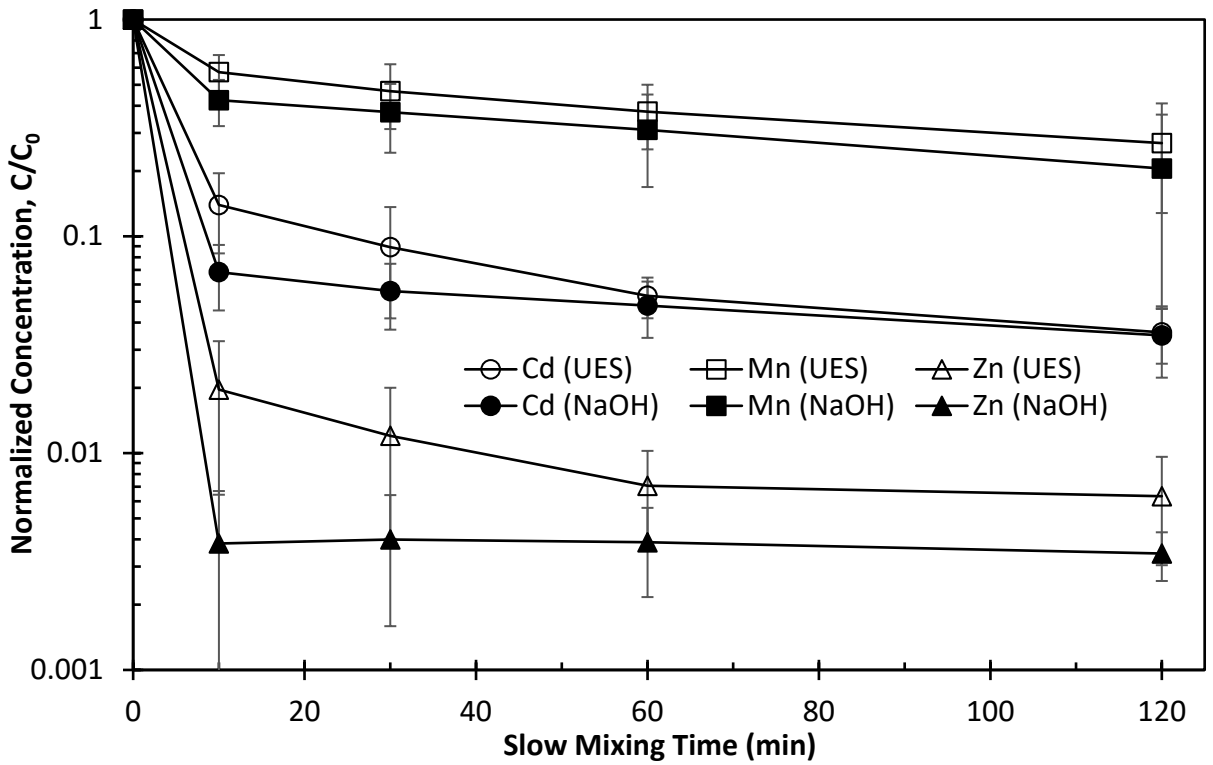

Figure 3. Normalized dissolved metals concentration as a function of slow mixing time in LMDT water. Error bars represent the standard deviation of triplicate jar tests. UES dose: 400 mg/L, NaOH dose: 100 mg/L, Cd0: 0.042±0.017 mg/L, Mn0: 2.8±1.3 mg/L, Zn0: 7.2±2.8 mg/L.

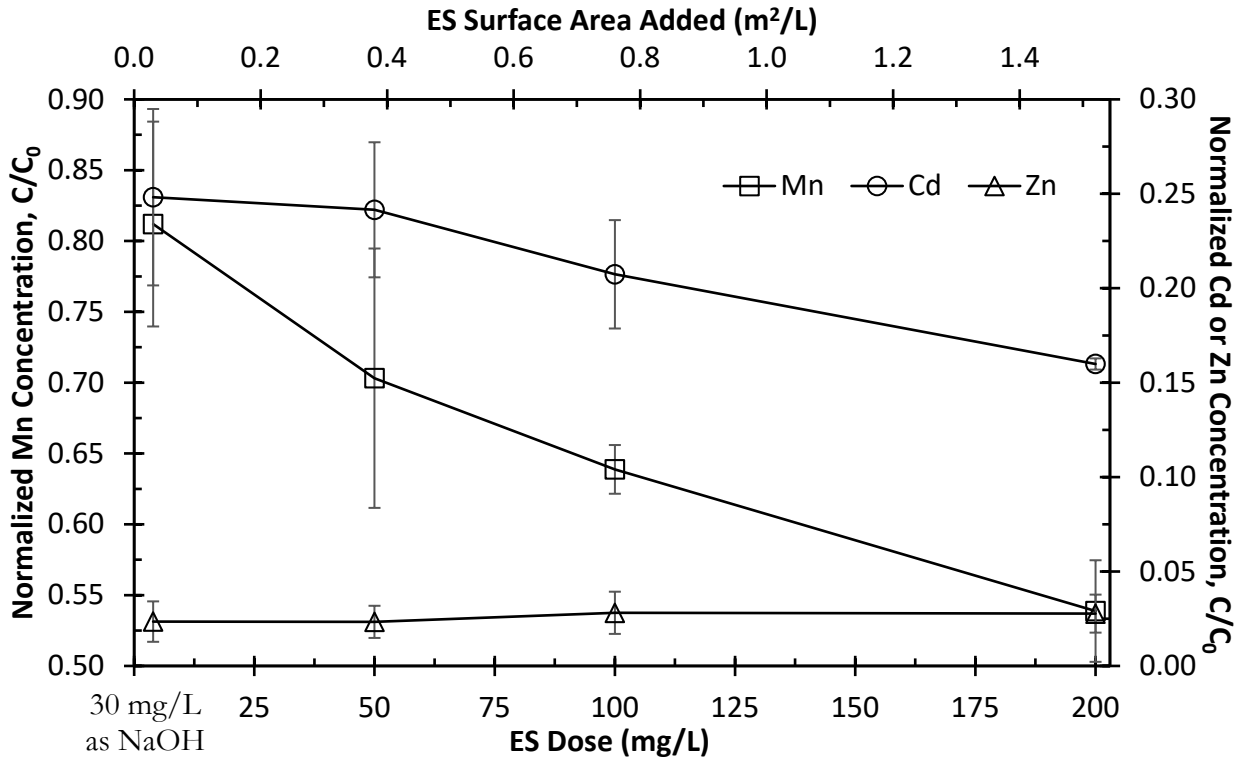

Figure 4. Normalized dissolved metals concentrations as a function of ES dose and surface area added in LMDT water. Error bars represent the standard deviation of triplicate jar tests. NaOH dose (all jars): 30 mg/L, initial pH: 7.7±0.2, final pH (all jars): 9.4±0.1, Cd0=0.0048±0.00044 mg/L, Mn0=0.46±0.095 mg/L, Zn0=1.2±0.013 mg/L.

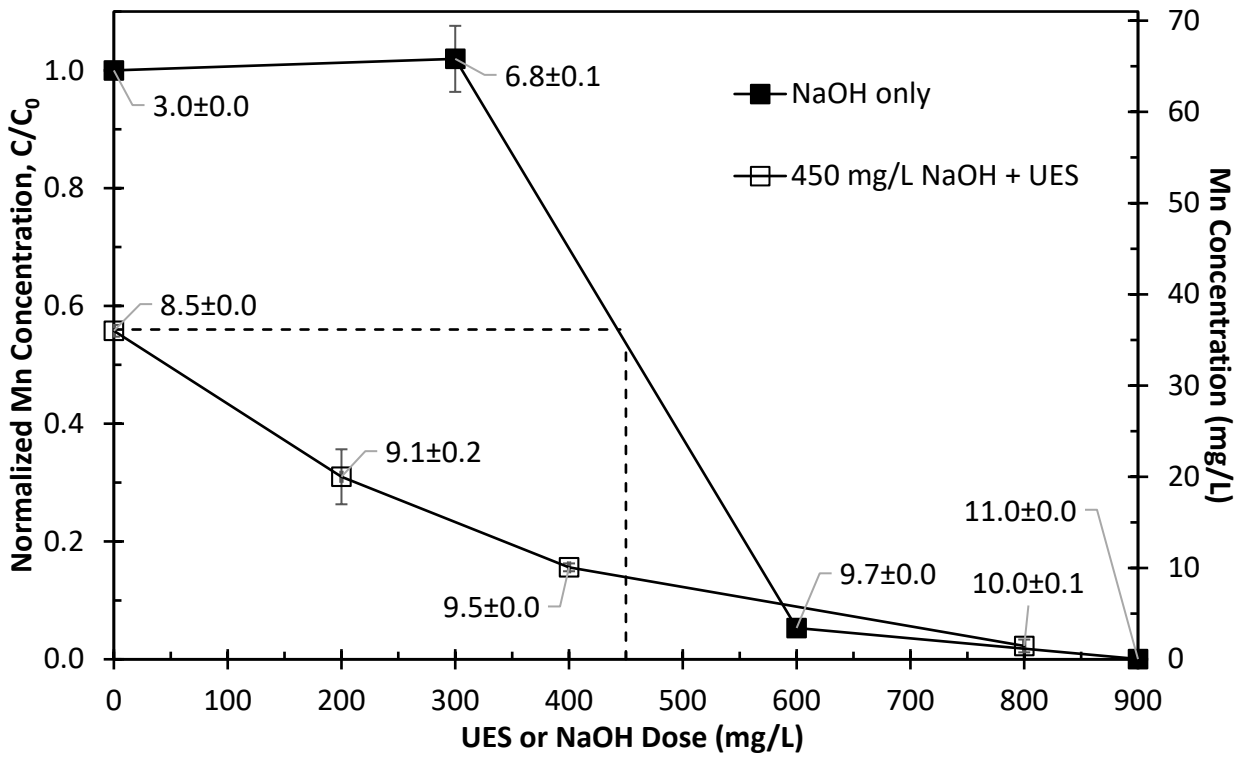

Figure 5. Normalized dissolved Mn concentration (Mn0=65±1.9 mg/L) as a function of (a) NaOH dose only and (b) combination of constant NaOH dose (450 mg/L) with varying amounts of UES in AT water. Error bars represent the standard deviation of duplicate jar tests. Called out values are final pH.

Tables

Table 3. Raw water quality range during testing.

Parameter	Value Range		Units
	LMDT	AT	
Alkalinity	90 – 150	0	mg/L as $CaCO_3$
Hardness	280 – 390	NM	mg/L as $CaCO_3$
ORP	200 – 500	NM	mV
pH	6.8 – 7.9	2.9 – 3.0	su
Cd	0.0043 – 0.053	0.070 – 0.088	mg/L
Mn	0.089 – 4.1	60 – 82	mg/L
Zn	1.2 – 9.3	30 – 38	mg/L

[a]NM – not measured. [b]ORP – oxidation reduction potential relative to the standard hydrogen electrode (SHE).

Table 2. *Relative EDS mass percent values for slag surfaces before and after testing with LMDT water at a dose of 400 mg/L (UES only) and 200 mg/L (ES with 30 mg/L NaOH).*

Element	UES		ES			
	Unused	Used	Ca-Dominated Particles		Fe-Dominated Particles	
			Unused	Used	Unused	Used
Al	0.9±0.4^{A}	0.7±0.0^{A}	1.7±0.5^{A}	1.6±0.6^{A}	1.1±0.1^{A}	0.8±0.2^{A}
C	4.3±1.1^{AB}	9.5±2.0^{C}	4.3±0.6^{AB}	6.2±0.6^{BC}	3.6±1.2^{AB}	2.8±1.1^{A}
Ca	34.2±6.3^{A}	27.5±5.2^{AB}	27.1±3.9^{AB}	22.3±5.0^{B}	4.6±1.9^{C}	6.0±0.8^{C}
Cd	NDP	NDP	NDP	NDP	NDP	NDP
Cr	NDP	NDP	0.2±0.1^{A}	0.2±0.0^{A}	0.1±0.3^{A}	0.8±0.5^{A}
Fe	5.4±2.9^{A}	5.1±2.7^{A}	12.2±4.1^{A}	11.2±0.4^{A}	48.6±0.6^{B}	49.2±13.3^{B}
Mg	1.0±0.6^{A}	2.0±1.7^{A}	3.3±2.3^{A}	1.8±0.7^{A}	1.7±1.8^{A}	2.7±0.6^{A}
Mn	0.4±0.2^{A}	0.6±0.3^{A}	1.3±0.4^{A}	1.3±0.3^{A}	1.9±1.2^{AB}	3.5±1.1^{B}
O	47.2±3.0^{A}	48.8±2.6^{A}	40.5±1.1^{AB}	45.0±1.7^{A}	34.2±5.2^{AB}	28.0±12.2^{B}
P	0.1±0.0^{A}	0.1±0.0^{A}	0.4±0.1^{BC}	0.5±0.1^{C}	0.3±0.2^{ABC}	0.2±0.1^{AB}
S	0.0±0.1^{A}	0.2±0.0^{B}	0.0±0.0^{A}	0.1±0.1^{A}	NDP	0.0±0.0^{A}
Si	6.4±2.6^{ABC}	4.8±0.8^{ABC}	8.7±1.9^{C}	7.1±2.0^{BC}	3.2±1.2^{AB}	2.4±0.8^{A}
Ti	0.1±0.2^{A}	0.1±0.0^{A}	0.3±0.3^{AB}	0.3±0.1^{AB}	0.8±0.7^{AB}	1.0±0.2^{B}
Zn	NDP	0.6±0.2^{A}	NDP	2.5±1.7^{AB}	NDP	2.7±0.3^{B}

[a]Values are average±standard deviation for three (n=3) chosen slag particles. [b]NDP – no discernable peak in EDS spectrum, value taken as 0.0±0.0 for statistical analysis. [c]Values that do not share a letter across rows are significantly different at the 95% confidence level.